CellPress

Current Biology
Article

Late rDNA Condensation Ensures Timely Cdc14 Release and Coordination of Mitotic Exit Signaling with Nucleolar Segregation

Ana Isabel de los Santos-Velázquez,[1,2] Inés G. de Oya,[1,2] Javier Manzano-López,[1,2] and Fernando Monje-Casas[1,3,*]
[1]Centro Andaluz de Biología Molecular y Medicina Regenerativa (CABIMER), Spanish National Research Council (CSIC), University of Seville, and University Pablo de Olavide, Avda. Américo Vespucio 24, 41092 Sevilla, Spain
[2]These authors contributed equally
[3]Lead Contact
*Correspondence: fernando.monje@cabimer.es
https://doi.org/10.1016/j.cub.2017.09.028

SUMMARY

The nucleolus plays a pivotal role in multiple key cellular processes. An illustrative example is the regulation of mitotic exit in *Saccharomyces cerevisiae* through the nucleolar sequestration of the Cdc14 phosphatase. The peculiar structure of the nucleolus, however, has also its drawbacks. The repetitive nature of the rDNA gives rise to cohesion-independent linkages whose resolution in budding yeast requires the Cdc14-dependent inhibition of rRNA transcription, which facilitates condensin accessibility to this locus. Thus, the rDNA condenses and segregates later than most other yeast genomic regions. Here, we show that defective function of a small nucleolar ribonucleoprotein particle (snoRNP) assembly factor facilitates condensin accessibility to the rDNA and induces nucleolar hyper-condensation. Interestingly, this increased compaction of the nucleolus interferes with the proper release of Cdc14 from this organelle. This observation provides an explanation for the delayed rDNA condensation in budding yeast, which is necessary to efficiently coordinate timely Cdc14 release and mitotic exit with nucleolar compaction and segregation.

INTRODUCTION

The nucleolus forms around the rDNA genes, which are arranged as a cluster of tandemly repeated units [1, 2]. The rDNA repeats are transcribed by the RNA polymerase I (Pol I), which generates an initial pre-rRNA precursor that is cleaved and post-transcriptionally modified with the help of small nucleolar ribonucleoprotein particles (snoRNPs) and other processing factors to give rise to the mature rRNAs. Central components of the snoRNPs are the small nucleolar RNAs (snoRNAs), a large class of non-coding RNAs that guide sequence-specific chemical modifications of the pre-rRNA and its post-transcriptional processing [3, 4]. The snoRNAs are classified into two types, C/D box and H/ACA box, and they work in close association with the core proteins of the snoRNPs, which differ for both classes of snoRNAs and include the enzymes that mediate the modifications that each catalyze in the pre-rRNA [3, 4]. The assembly of the final snoRNP is a complex process that requires many factors [5]. Among them, Rsa1/NUFIP1 plays a central role in the assembly of C/D box snoRNPs by mediating the interaction between the core protein Snu13/15.5K and the Rvb1/p55 and Rvb2/p50 components of the Hsp82/Hsp90 co-chaperone R2TP complex [6, 7].

Historically, the nucleolus has been primarily associated with its function in ribosome biogenesis. However, this organelle plays key roles in a variety of other fundamental processes [1, 8]. The capacity of the nucleolus to specifically retain certain molecules is a commonly employed strategy that cells use to regulate these processes [1, 8, 9]. A classic example is the regulation of mitotic exit in budding yeast through the control of the localization of the Cdc14 phosphatase [10–12]. Cdc14 is sequestered in the nucleolus from G1 to metaphase through its binding to Cfi/Net1 [11, 12]. However, at the metaphase-to-anaphase transition, Cdc14 is first released toward the nucleus and then, later during anaphase, also to the cytoplasm, where it triggers mitotic exit by promoting the inactivation of mitotic cyclin-dependent kinase (CDK) activity [10, 13]. The initial nucleolar release of Cdc14 is facilitated by the Cdc-fourteen early anaphase release (FEAR) network. Although not essential for cell viability, FEAR is critical for accurate chromosome segregation and the coordination of this process with key cell cycle events [10, 13]. Interestingly, FEAR function is of pivotal importance for the proper segregation of the nucleolus itself. In contrast to most parts of the genome, the rDNA repeats maintain cohesion-independent linkages after metaphase and segregate late during anaphase [14–16]. Faithful nucleolar segregation requires the Cdc14-mediated inhibition of Pol I-dependent rDNA transcription during early anaphase, which facilitates condensin loading on the rDNA and elimination of these linkages [17]. However, the reasons behind this differential regulation of rDNA condensation and the late nucleolar segregation are still unknown.

After its initial release, the Mitotic Exit Network (MEN) promotes the full liberation of Cdc14. This pathway is initiated by the Tem1 GTPase, whose activity is negatively regulated by Bfa1-Bub2 and promoted by the bud cortex-associated protein Lte1 [18–20]. Tem1 triggers a signaling cascade that includes the Cdc15 and Dbf2 kinases and allows a sustained Cdc14 release [18, 21–23]. In contrast to FEAR, MEN is

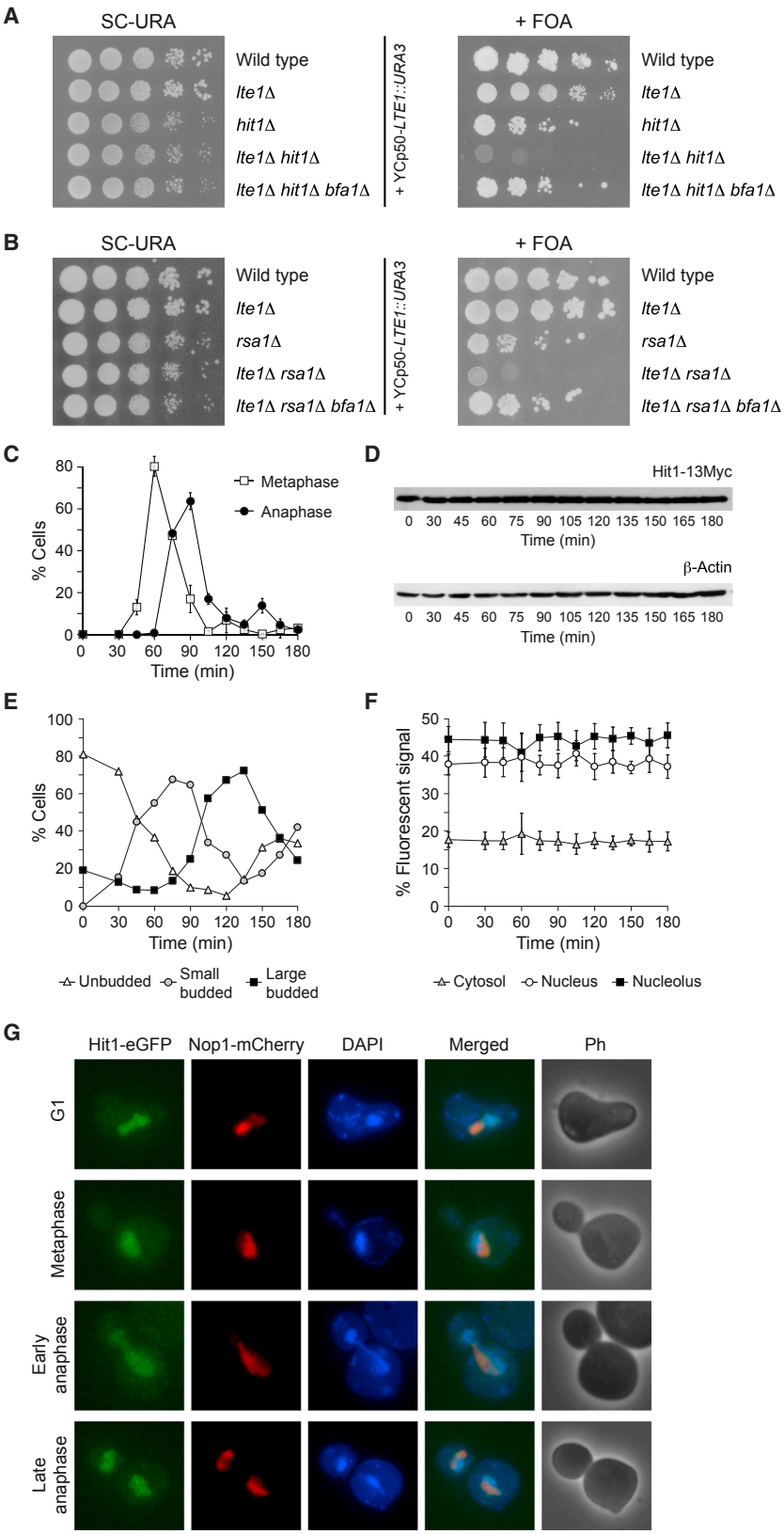

Figure 1. Hit1 Deficiency Leads to Synthetic Lethality with *lte1*Δ

(A and B) Cells carrying the YCp50-*LTE1* plasmid (F1312, F527, F2065, F2061, and F2130 (A) or F1312, F527, F2665, F2614, and F2834 (B)) were plated by spotting 10-fold serial dilutions of a culture (OD_{600} = 0.5) on minimal medium, without uracil (SC-URA) or containing 0.3 mg/mL FOA (+FOA), and incubated at 23°C.

(C and D) Wild-type cells expressing Hit1-13Myc (F1389) were grown in YPD at 26°C, arrested in G1 with 5 μg/mL α-factor, and then released into YPD without pheromone at 26°C. (C) Percentages of metaphase and anaphase cells are shown, as determined by the analysis of spindle and nuclear morphologies. Error bars represent SD (n = 3). (D) Hit1-13Myc levels were analyzed by western blot. β-actin levels were used as a loading control.

(E–G) Wild-type cells expressing Hit1-EGFP and Nop1-mCherry (F1744) were grown in YPD at 30°C, blocked in G1 with 5 μg/mL α-factor, and released into YPD without pheromone at 30°C. (E) Cell cycle progression is shown, as determined by the percentage of unbudded, small-budded, and large-budded cells. (F) Percentage of total Hit1-EGFP fluorescent signal in the cytosol, nucleus, and nucleolus is shown. Error bars represent SD (n = 20). (G) Representative images display Hit1-EGFP (green) and Nop1-mCherry (red) localization, the morphology of the nucleus (DAPI, blue), a phase-contrast (Ph) image and a merged image.

See also Figures S1 and S2.

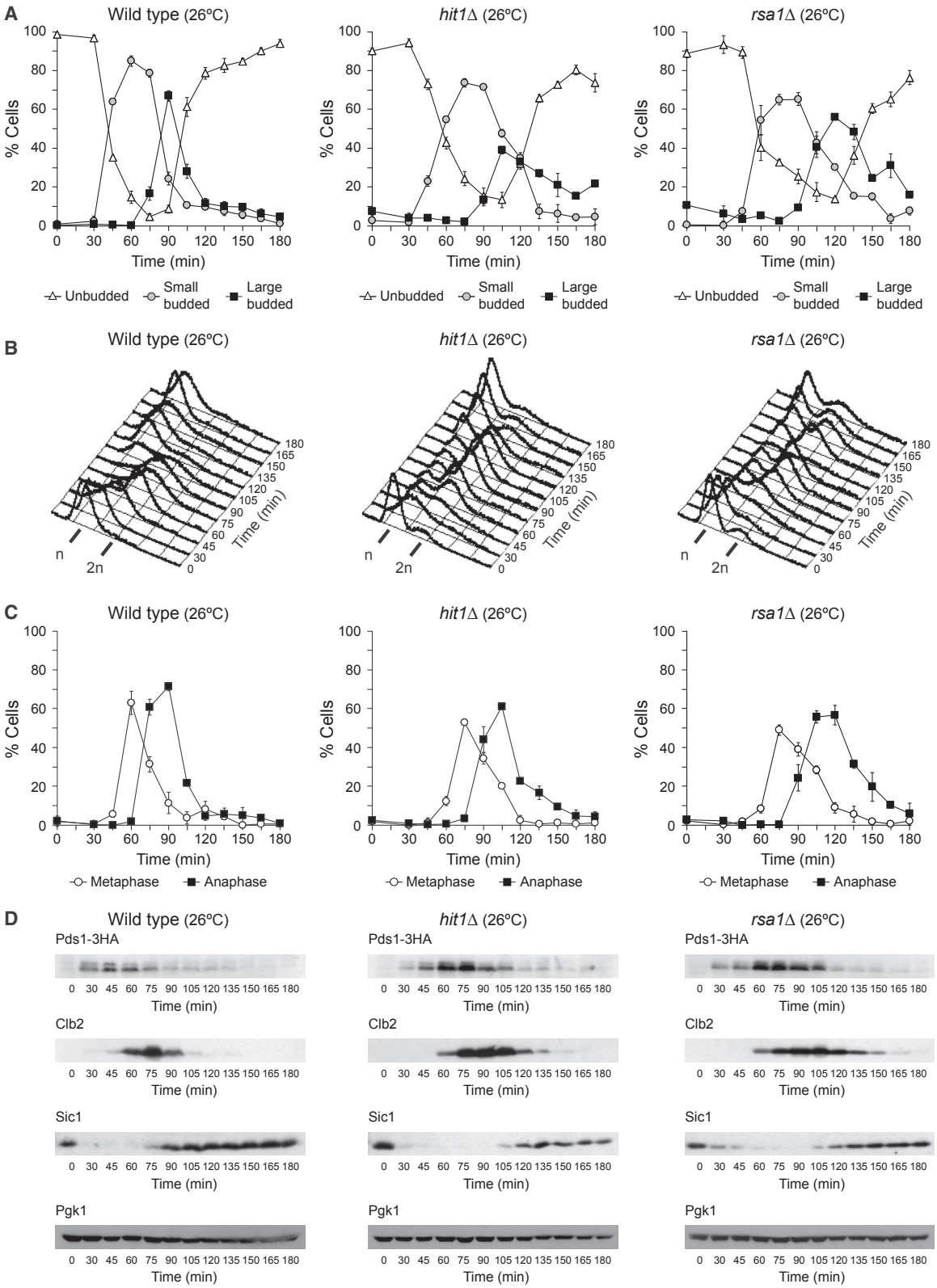

Figure 2. Hit1-Rsa1 Deficiency Impairs Cell Cycle Progression

Cells expressing Pds1-3HA (F1586, F1423, and F3285) were grown in YPD at 23°C, arrested in G1 with 5 μg/mL α-factor, and released into YPD medium without pheromone at 26°C. See also Figure S3.

(legend continued on next page)

essential and strictly required for the completion of mitosis [10]. However, the contribution of the FEAR pathway to the proper regulation of mitotic exit is not to be disregarded. As such, FEAR becomes indispensable for cell viability in the absence of Lte1 [24].

Hit1 is a C/D box snoRNP assembly factor that acts in a complex with Rsa1, and it is required to maintain steady-state levels of this protein in budding yeast, a function that seems to be conserved [25]. Interestingly, simultaneous deletion of the *HIT1* and *LTE1* genes leads to synthetic lethality [24], which suggests that the lack of Hit1 could interfere with the functionality of FEAR. Here, we uncover a new link between rRNA-associated factors and the regulation of mitotic exit by demonstrating that the lack of Hit1-Rsa1 determines nucleolar hyper-condensation, which compromises timely Cdc14 release. Importantly, our results provide an answer to the long-standing question of why the rDNA segregates later than most regions of the *S. cerevisiae* genome.

RESULTS

Simultaneous *HIT1* and *LTE1* Deletion Leads to Synthetic Lethality that Is Rescued by Bfa1 Inactivation

Hit1 is a snoRNP assembly factor that contributes to C/D box snoRNA stability [25]. Interestingly, simultaneous deletion of *HIT1* and *LTE1* (the gene encoding the MEN activator) leads to synthetic lethality [24], which suggests that lack of Hit1 could interfere with the functionality of the FEAR pathway. The synthetic lethality associated with simultaneous deficiency of both Lte1 and a factor that compromises Cdc14 early anaphase release is determined by the inability of the cells to promote mitotic exit, and it can be rescued by the deletion of *BFA1*, which encodes a MEN inhibitor [26]. To evaluate whether this was the case for Hit1, we generated *S. cerevisiae hit1*Δ *lte1*Δ cells also carrying the YCp50-*LTE1* centromeric plasmid, which contains a wild-type copy of both *LTE1* and the *URA3* gene [27], and we analyzed their capacity to grow in medium containing 5-fluorotic acid (FOA), which prevents the growth of *URA3* cells [28]. Remarkably, in contrast to wild-type (W303, *ura3-1*), *hit1*Δ, or *lte1*Δ cells carrying YCp50-*LTE1* and according with the simultaneous lack of *HIT1* and *LTE1* being synthetically lethal, *hit1*Δ *lte1*Δ YCp50-*LTE1* cells were unable to lose the plasmid and grow in medium with FOA (Figure 1A). Furthermore, the capacity of *hit1*Δ *lte1*Δ YCp50-*LTE1* cells to grow in FOA was restored by the additional deletion of *BFA1*, which suggests that the synthetic lethality is likely associated with defective Cdc14 function and, hence, the inability to promote mitotic exit (Figure 1A). Similar results were obtained when *LTE1* was inactivated using a glucose-repressible promoter (Figure S1A). Also accordingly, and as previously shown for mutations that compromise FEAR function [29], *hit1*Δ impaired the viability at semi-permissive temperatures of cells carrying *tem1-3*, a thermosensitive allele of the MEN-initiating GTPase [18] (Figure S1B).

Hit1 is functionally linked with Rsa1, with whom it forms a complex [25]. Remarkably, *rsa1*Δ *lte1*Δ YCp50-*LTE1* cells were also unable to grow in FOA unless *BFA1* was additionally deleted in this background (Figure 1B). Therefore, our results indicate that it is the loss of function of Hit1-Rsa1, and not an independent specific feature of Hit1-deficient mutants, that determines the synthetic lethality in cells that also lack Lte1.

To evaluate how Hit1 deficiency could interfere with the early anaphase release of Cdc14, we first analyzed the levels and localization of Hit1 during the cell cycle. In cells released from a G1 arrest and allowed to synchronously progress into mitosis, Hit1 levels remained constant throughout the cell cycle (Figures 1C and 1D). Remarkably, and although localization of Hit1 did not change either, the protein was permanently found both in the nucleus and nucleolus of the cells, despite the nucleolar marker used (Figures 1E–1G; Figures S1C–S1E). This places Hit1 in an optimal sub-cellular location for a factor that could affect Cdc14 release. Similar results were obtained with Rsa1 (Figures S1F–S1M). Hit1 is required to maintain steady-state levels of Rsa1 [25] (Figures S2A and S2B). Interestingly, *rsa1*Δ cells also showed reduced levels of Hit1 (Figures S2C and S2D). However, while nuclear and nucleolar localization of Hit1 was severely affected in *rsa1*Δ cells (Figure S2E), Rsa1 still localized to both compartments in cells lacking *HIT1* (Figure S2F), which suggests that, despite being interdependent for their expression, it is Rsa1 that determines localization of the complex. This is in agreement with the fact that only Rsa1 seems to bear a clear nuclear localization signal [25].

HIT1 Deletion Impairs Mitotic Exit

We next analyzed cell cycle progression in wild-type and *hit1*Δ cells that were first arrested in G1 and then allowed to synchronously enter the cell cycle at 26°C. Deletion of *HIT1* caused an overall delay in cell cycle progression (Figures 2A–2D). Despite this general delay, while *hit1*Δ cells accumulated in metaphase approximately only 15 min later than the wild-type (Figure 2C), the *hit1*Δ mutant then completed the metaphase-to-anaphase transition and exited mitosis with a substantially longer delay, as estimated by the analysis of Pds1 (securin, degraded at the metaphase-to-anaphase transition [30]), Clb2 (a cyclin degraded during mitotic exit [31]), and Sic1 (a CDK inhibitor [31]) (Figure 2D). Similar results were obtained when cell cycle progression was analyzed in *rsa1*Δ cells (Figure 2). Importantly, the initial delay in Pds1 degradation in *hit1*Δ cells, and, therefore, in the initiation of the metaphase-to-anaphase transition, was not associated with defects in prior cell cycle stages as a consequence of the activation of the DNA damage or the spindle assembly checkpoints (Figures 3A and 3B). Hence, our results are in agreement with the lack of Hit1-Rsa1, besides interfering with other cell cycle stages, specifically impairing mitotic exit.

Hit1 was originally described as an essential gene for growth at high temperatures (hence its name, high-temperature growth 1) [32, 33], which contrasts with the cold-sensitive

(A) Cell cycle progression as determined by the percentage of unbudded, small-budded, and large-budded cells. Error bars represent SD (n = 3).
(B) DNA content estimated by fluorescence-activated cell sorting (FACS) analysis.
(C) Analysis of cell cycle progression based on spindle and nuclear morphologies. Percentages of metaphase and anaphase cells are shown. Error bars represent SD (n = 3).
(D) Pds1-3HA, Clb2, and Sic1 levels were analyzed by western blot. Pgk1 levels were used as a loading control.

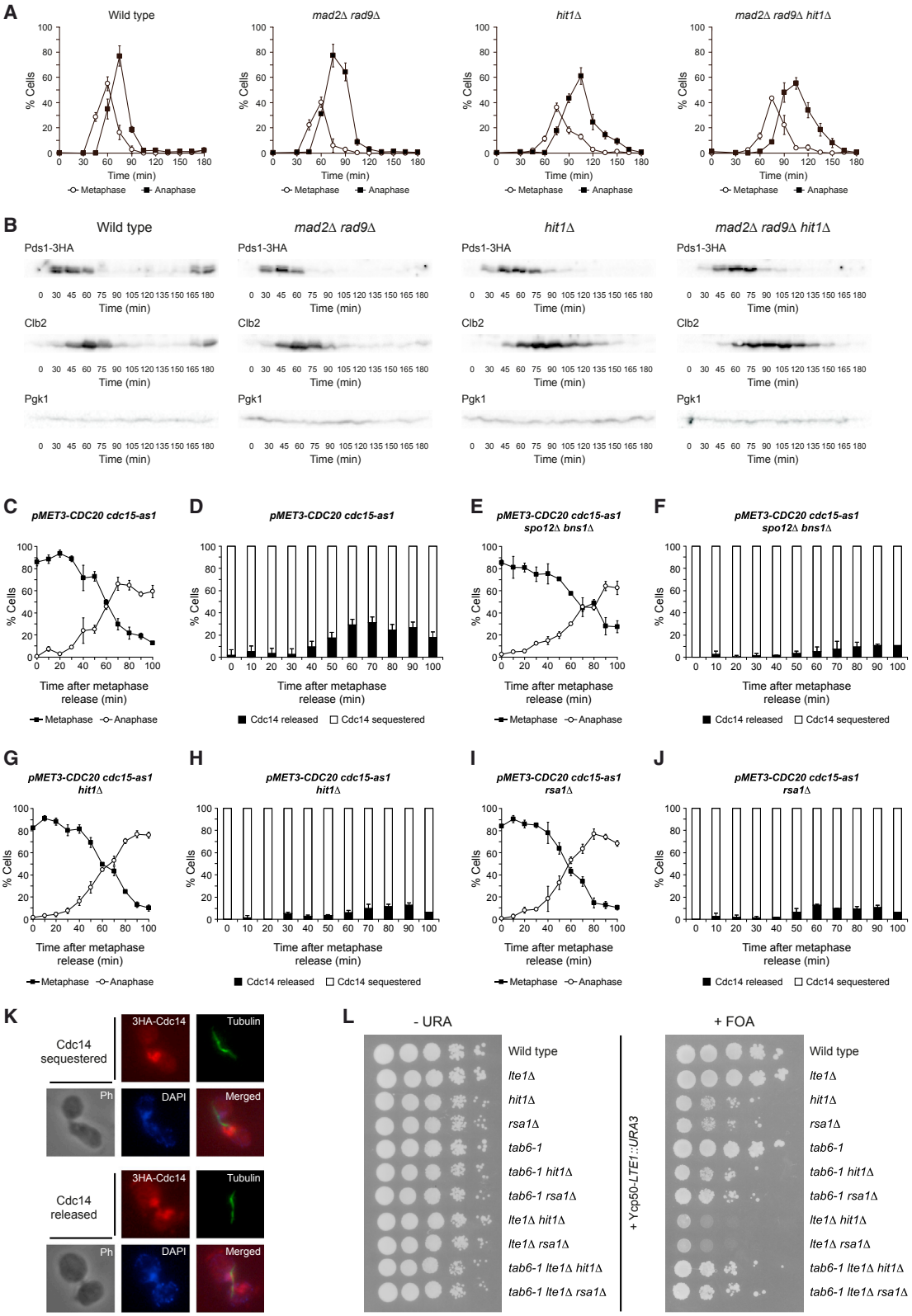

Figure 3. Lack of Hit1-Rsa1 Impairs Cdc14 Early Anaphase Release

(A and B) Cells expressing Pds1-3HA (F1586, F3635, F1423, and F3636) were grown in YPD at 23°C, arrested in G1 with 5 μg/mL α-factor, and released into YPD medium without pheromone at 26°C. (A) Analysis of cell cycle progression based on spindle and nuclear morphologies is shown. Percentages of metaphase and

(legend continued on next page)

phenotype of *lte1*Δ cells [34] (Figure S3A). Deletion of *HIT1* or *RSA1*, however, had a similar impact on cell cycle progression both at 26°C and 37°C (Figures S3B–S3E), which suggests that the thermosensitivity of *hit1*Δ cells is associated with additional problems not specifically linked to a defective regulation of cell cycle progression. This is in agreement with Hit1-Rsa1 carrying out different functions in the cells that are distinctively affected by the temperature, hence making it difficult to assign the cause of this temperature-sensitive phenotype [35, 36]. Subsequently, we carried out the characterization of the consequences of the lack of Hit1-Rsa1 on mitotic exit at 26°C, unless otherwise indicated.

Hit1 overexpression also impaired cell viability. However, in contrast to *HIT1* deletion, elevated Hit1 levels affected cell growth at all temperatures tested (Figure S4A). Furthermore, increased levels of Hit1 or Rsa1 did not seem to affect cell cycle progression, and, contrary to overexpression of the FEAR component Spo12 [29], they did not rescue the lethality associated with *tem1-3* at semi-permissive temperatures (Figures S4B, S4D, S4F, and S4H). This strongly suggests that increased levels of Hit1-Rsa1 do not only impair cell viability by interfering with Cdc14 function but also as a consequence of other unrelated problems.

Lack of Hit1-Rsa1 Compromises Cdc14 Early Anaphase Release

Our previous results suggested that Hit1-Rsa1 could be important for the initial liberation of Cdc14. Therefore, we analyzed the dynamics of Cdc14 release in *hit1*Δ and *rsa1*Δ cells during the metaphase-to-anaphase transition. Since *HIT1* or *RSA1* deletion caused a general cell cycle delay that was already evident before metaphase (Figure 2), we first arrested cells at this cell cycle stage by conditionally inactivating the anaphase-promoting complex cofactor Cdc20 [31], and then we followed Cdc14 localization as cells synchronously entered the metaphase-to-anaphase transition after Cdc20 reactivation. To this end, cells carried the *CDC20* gene under control of the methionine-repressible *MET3* promoter (*pMET3-CDC20*). Additionally, cells carried the *cdc15-as1* allele, which encodes an ATP analog-sensitive Cdc15 kinase [37]. Cdc15 inactivation prevents the MEN-dependent Cdc14 release in late anaphase, so that only the partial and transient FEAR-induced release of the phosphatase during early anaphase can be observed [38], thus facilitating evaluation of the specific impact of *hit1*Δ on this process. As expected, *pMET3-CDC20 cdc15-as1* cells transitorily released Cdc14 into the nucleus as they exited the Cdc20-dependent metaphase block, although the phosphatase was then re-sequestered as a result of the inhibition of MEN due to Cdc15 inactivation (Figures 3C, 3D, and 3K). This transient Cdc14 release was not observed in *pMET3-CDC20 cdc15-as1* cells when FEAR was inactivated by simultaneous *SPO12* and *BNS1* deletion [38] (Figures 3E and 3F). Remarkably, *HIT1* or *RSA1* deletion also impaired the Cdc14 early anaphase release in *pMET3-CDC20 cdc15-as1* cells (Figures 3G–3J). Furthermore, and similar to what was observed for the *spo12*Δ *bns1*Δ mutant, Pds1 degradation was also significantly delayed in *hit1*Δ and *rsa1*Δ cells released from the metaphase arrest when compared to the wild-type, in agreement with these mutants not efficiently inducing the Cdc14-dependent feedback loop that enhances securin degradation [39] (Figure S4I).

Finally, we also analyzed whether the synthetic lethality caused by simultaneous deletion of *HIT1* or *RSA1* and *LTE1* could be rescued by actively facilitating the nucleolar release of Cdc14. The *tab6-1* allele encodes a mutant Cdc14 protein with reduced affinity for Cfi1/Net1 [40], which is prematurely found out of the nucleolus but does not affect rDNA segregation or condensation (Figures S4J–S4R). Notably, *tab6-1* allowed both *hit1*Δ *lte1*Δ YCp50-*LTE1* and *rsa1*Δ *lte1*Δ YCp50-*LTE1* cells to grow in FOA (Figure 3L), which further demonstrates that the synthetic lethality of *hit1*Δ *lte1*Δ and *rsa1*Δ *lte1*Δ cells is caused by their incapacity to efficiently promote Cdc14 nucleolar liberation.

HIT1 or *RSA1* Deletion Promotes Nucleolar Hyper-condensation

To unveil the mechanisms by which lack of Hit1-Rsa1 impairs mitotic exit, we first analyzed whether Hit1 and Cdc14 can directly interact using bimolecular fluorescence complementation (BiFC) assays [41]. As a control, we initially corroborated that Cdc14 and Cfi/Net1, whose association has been widely established by other means [11, 12], strongly interacted and gave rise to a fluorescent signal that localized to the nucleolus (Figures S5A and S5B). Remarkably, a fusion of Hit1 with the Venus fluorescent protein N-terminal domain (VN) strongly interacted with the nucleolar protein Nop1 fused to the C-terminal Venus domain (VC), and it generated a fluorescent signal restricted to the nucleolus (Figures S5A, S5C, and S5D). This indicates that Hit1-VN was correctly expressed and localized, in contrast to Hit1-VC, which seemed not to be functional (Figure S5A). Interestingly, the in vivo Hit1-Nop1 interaction had not been previously described, although it is in agreement with the isolation of Nop1 in tandem affinity purifications using Hit1-TAP [25]. This interaction is not cell cycle regulated (Figure S5C), which is congruent with Hit1 being permanently found

anaphase cells are shown. Error bars represent SD (n = 3). (B) Pds1-3HA and Clb2 levels were analyzed by western blot. Pgk1 levels were used as a loading control.

(C–K) Cells carrying *cdc15-as1*, *pMET3-CDC20*, and *3HA-CDC14* alleles (F2073, F2508, F2205, and F3410) were grown in minimal medium without methionine at 26°C, arrested in G1 with 7.5 μg/mL α-factor, and released into minimal medium without pheromone and with 10 mM methionine at 26°C. Once blocked in metaphase (t = 0 min), cells were released into minimal medium without methionine and with 20 μM 1-NA-PP1. (C, E, G, and I) Cell cycle progression was determined based on spindle and nuclear morphologies. Percentages of metaphase and anaphase cells are shown. Error bars represent SD (n = 3). (D, F, H, and J) Percentage of cells displaying 3HA-Cdc14 sequestered (white bars) or released (black bars) from the nucleolus is shown. Error bars represent SD (n = 3). (K) Representative images display Cdc14 localization (red). Tubulin (green), nuclear morphology (DAPI, blue), a phase-contrast (Ph) image, and a merged image are also shown.

(L) Cells carrying the YCp50-*LTE1* plasmid (F1312, F527, F2065, F2665, F2602, F2603, F3459, F2061, F2614, F2601, and F3461) were plated by spotting 10-fold serial dilutions of a culture (OD_{600} = 0.5) on minimal medium, without uracil (−URA) or containing 0.3 mg/mL FOA (+FOA), and incubated at 23°C.

See also Figure S4.

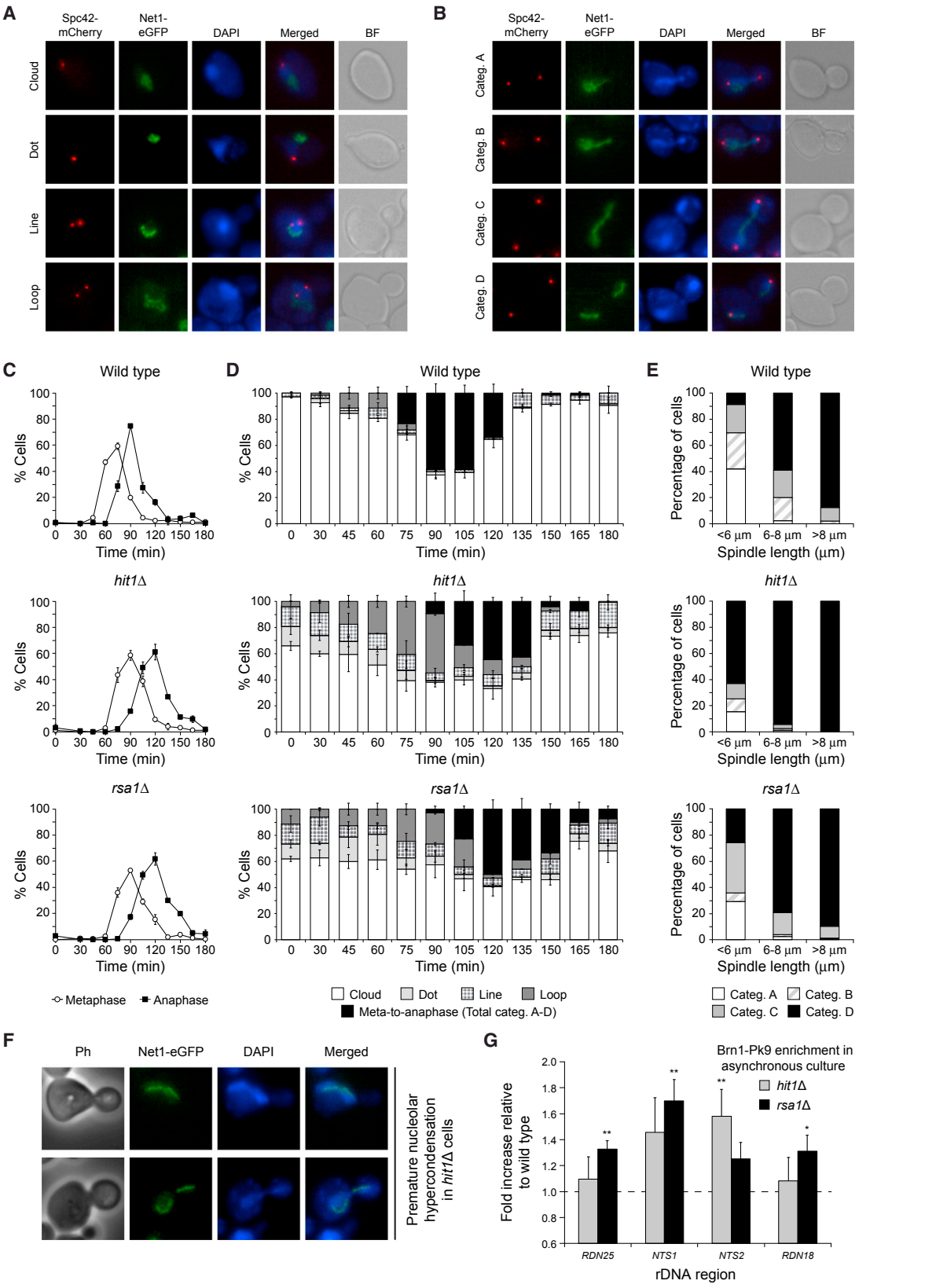

(legend on next page)

in the nucleolus (Figures 1E–1G). In contrast to the strong Hit1-Nop1 interaction, cells showed either non-detectable or very weak fluorescent nucleolar signal when the putative interactions between Hit1-VN and either Cdc14-VC or Net1-VC were analyzed (Figures S5A and S5E). Since we were also unable to co-immunoprecipitate Hit1 with Cdc14, our results suggest either that Hit1 does not directly interact with Cdc14 or that this interaction is really transient or weak. Finally, and although phosphorylation of Cdc14 and Net1, which promotes Cdc14 release [42], was delayed in *hit1*Δ cells in agreement with their slower cell cycle progression, no evident differences in the phosphorylation levels of these proteins were observed in this mutant when compared to the wild-type (Figures S5F and S5G).

We next analyzed whether lack of Hit1 could interfere with the localization or function of FEAR components, such as Fob1 [27]. Interestingly, and although we did not observe any obvious defect in the localization of Fob1 to the nucleolus, the morphology of this organelle seemed to be abnormal in the *hit1*Δ mutant (Figures S6A and S6B). Specifically, the nucleolus appeared more compacted in *hit1*Δ cells than in the wild-type, which could be indicative of rDNA hyper-condensation. In budding yeast, the rDNA fully condenses in anaphase, later than most other genomic regions [14, 15, 43, 44]. Compaction of the rDNA locus can be analyzed by visualizing a fluorescently tagged version of the rDNA-binding protein Cfi1/Net1 [16, 44–46]. In G1, the nucleolus of wild-type cells displays a characteristic puff-like uncondensed appearance [43, 45] (cloud, Figure 4A). Then, as the cells progress through the cell cycle, the rDNA gets gradually more condensed until it finally adopts a characteristic line-like appearance once maximal nucleolar condensation is achieved [43–46] (Figures 4A–4D). Remarkably, both *hit1*Δ and *rsa1*Δ cells displayed nucleolar morphologies associated with more condensed forms of the rDNA already from G1 to metaphase (Figures 4C, 4D, and S6D).

Next, we more carefully compared the kinetics of rDNA condensation in *hit1*Δ and *rsa1*Δ cells as they transited from metaphase to anaphase. According to previous analyses of this transition [46], cells were classified into four categories (A to C [anaphase bridges] and D) that were representative of different stages of rDNA condensation (Figure 4B), from a less condensed bridge morphology (category A) to the most condensed line-like appearance observed once both copies of the rDNA separate (category D). As suggested by our previous observations, the rDNA locus was prematurely hyper-condensed in both *hit1*Δ and *rsa1*Δ cells, with an elevated percentage of cells already displaying maximal rDNA compaction at spindle lengths shorter than 6 μm and an overall reduced nucleolar size (Figures 4E, 4F, S6D, and S6E). These results were very similar when nucleolar morphology was analyzed using Fob1 (Figures S6A–S6C), another bona fide rDNA marker [16, 44]. The increase in nucleolar condensation was not observed in *spo12*Δ *bns1*Δ cells, indicating that this phenotype is not shared by all mutants affected in Cdc14 early anaphase release (Figures S6F–S6K). Importantly, we did not observe visible defects in spindle morphology or elongation in the *hit1*Δ and *rsa1*Δ mutants during the metaphase-to-anaphase transition (Figures S6L–S6N), which, together with the fact that rDNA hyper-condensation was evident in these mutants even before spindle elongation was initiated as cells exited metaphase (Figures 4C and 4D), rules out that increased nucleolar compaction in *hit1*Δ and *rsa1*Δ cells could be instead explained by alterations in the kinetics of spindle extension that could provide more time for rDNA condensation to occur. Furthermore, increased nucleolar compaction was also not due to shortening of the rDNA array length in the *hit1*Δ and *rsa1*Δ mutants (Figure S7A). Finally, increased Hit1 and Rsa1 levels induced a mild decompaction of the rDNA, further supporting that normal levels of both proteins are essential to ensure proper nucleolar condensation (Figures S4B–S4G).

According with our previous analyses, cells lacking *HIT1* or *RSA1* showed increased association of the non-SMC condensin subunit Brn1 with the rDNA (Figure 4G). It is worth noting that even 2-fold changes in condensin levels can substantially affect nucleolar condensation [43]. Increased condensin association with the rDNA in both mutants was already observed from G1 to metaphase, also according with our previous observations (Figures S7B and S7C). We did not find differences in Brn1 loading on the rDNA in *hit1*Δ or *rsa1*Δ cells with respect to the wild-type during anaphase (Figure S7D), but this was expected since nucleolar condensation is maximum for wild-type cells at this stage. However, evaluation of the nucleolar release of the Smc4 condensin subunit, which can be used to analyze the kinetics of rDNA decondensation during mitotic exit [17, 47], indicated that deletion of either *HIT1* or *RSA1* caused persistent rDNA condensation in cells exiting from a *cdc15-as1*-induced anaphase arrest to a similar extent as when Pol I transcription was inhibited using rapamycin [47] (Figures S7E and S7F). Our results thus demonstrate that lack of Hit1-Rsa1 facilitates condensin accessibility to the rDNA, which determines nucleolar hyper-condensation.

Figure 4. Lack of Hit1-Rsa1 Leads to Nucleolar Hyper-condensation

(A–E) Cells expressing Spc42-mCherry and Net1-EGFP (F2301, F2303, and F3287) were grown in YPD with 300 μg/mL adenine at 23°C, arrested in G1 with 5 μg/mL α-factor, and released into fresh medium without pheromone at 26°C. (A and B) Representative images show cells for each of the pre-established categories of nucleolar compaction. Nuclear (DAPI, blue) and nucleolar (Net1-EGFP, green) morphologies, the SPBs (Spc42-mCherry, red), a bright-field (BF) image, and a merged image are shown. (C) Cell cycle progression was determined based on spindle and nuclear morphologies. Percentages of metaphase and anaphase cells are shown. Error bars represent SD (n = 3). (D) Percentage of cells within each of the nucleolar compaction categories is shown. Error bars represent SD (n = 3). (E) Percentage of cells within each of the categories (A–D) representative of the metaphase-to-anaphase transition are distributed according to spindle length.

(F) Representative examples of hyper-condensation in *hit1*Δ cells expressing Net1-EGFP (F2169). Besides Net1-EGFP (green), DAPI (blue), a phase-contrast (Ph) image, and a merged image are also shown.

(G) Condensin enrichment at different regions of the rDNA in wild-type (F2702), *hit1*Δ (F2730), and *rsa1*Δ (F3248) cells, as determined by chromatin immunoprecipitation with Brn1-Pk_9 and real-time PCR. Amplification efficiencies were normalized against the *TUB2* gene. Enrichment was calculated as the ratio between the input and the immunoprecipitated in the tagged strain relative to the same ratio in an untagged control (F496). Graphs represent fold increase relative to wild-type. Error bars represent SEM (n = 3). Statistically significant differences (**$p < 0.01$ and *$p < 0.05$), relative to the wild-type and according to a t test, are also shown. See also Figures S5–S7.

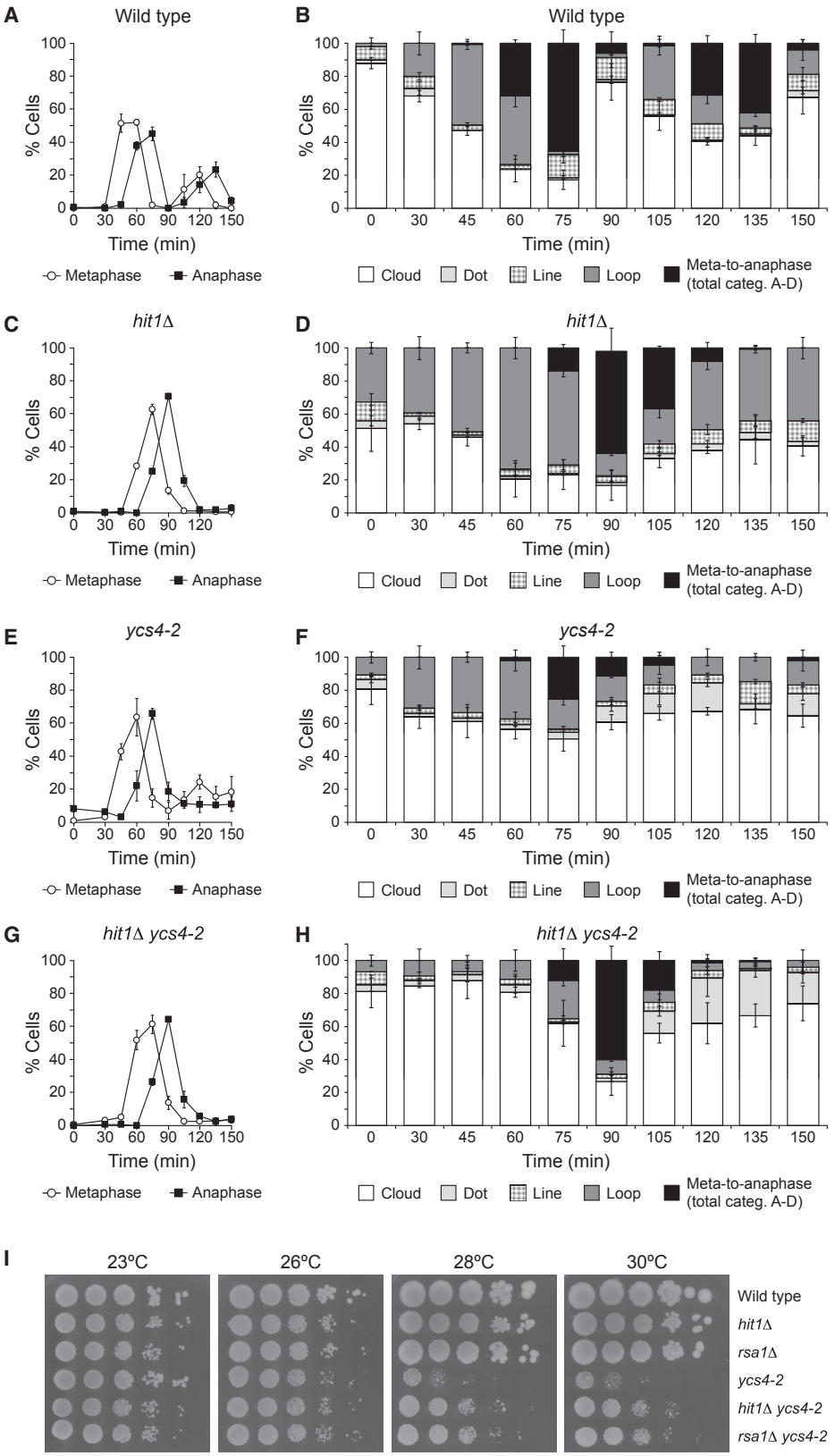

(legend on next page)

Deficient Cdc14 Early Anaphase Release in *hit1*Δ and *rsa1*Δ Cells Can Be Rescued by Alleviating Nucleolar Hyper-Condensation

Increased nucleolar compaction in *hit1*Δ cells could interfere with the FEAR-dependent Cdc14 release. If this were the case, alleviating nucleolar hyper-condensation should rescue the efficient release of the phosphatase during early anaphase in *hit1*Δ cells. To test this prediction, we used the *ycs4-2* allele, which encodes a thermolabile Ycs4 condensin subunit [48]. rDNA condensation is defective in the *ycs4-2* mutant even at permissive temperatures [49]. Remarkably, expression of this allele relieved the increased nucleolar condensation in *hit1*Δ cells (Figures 5A–5H). Furthermore, *HIT1* or *RSA1* deletion alleviated the growth defects shown by *ycs4-2* cells at semi-permissive temperatures (Figure 5I). Finally, we analyzed whether defective FEAR-dependent Cdc14 release in *hit1*Δ cells (Figures 3G and 3H) could be prevented by partially impairing condensin function with the *ycs4-2* allele. Excitingly, introduction of *ycs4-2* in *pMET-CDC20 cdc15-as1 hit1*Δ cells indeed restored early Cdc14 release at a semi-permissive temperature (Figures 6A and 6B).

In a *cdc14-1* mutant at the restrictive temperature, the rDNA fails to segregate because rRNA transcription by Pol I, which interferes with rDNA condensation, cannot be inhibited by Cdc14 [17]. In contrast, the rDNA segregates normally in a *cdc15-2* mutant despite the cells also arresting in anaphase due to MEN inactivation, since Cdc14 can be activated by the FEAR during the metaphase-to-anaphase transition [17]. Accordingly, the rDNA segregation defect in *cdc14-1* cells was abolished when Pol I-dependent transcription was inhibited with rapamycin, which induces nucleolar hyper-condensation (Figures 6C and 6D). Excitingly, increased rDNA condensation induced by *HIT1* or *RSA1* deletion also restored normal nucleolar segregation in this mutant background (Figures 6C and 6D), which improved the growth of *cdc14-1* cells at semi-permissive temperatures (Figure 6E). Hence, our results support that lack of Hit1-Rsa1 determines a hyper-condensation of the rDNA that impairs Cdc14 nucleolar release.

Lack of Hit1-Rsa1 Promotes Nucleolar Hyper-Condensation by Interfering with RNA Pol I Activity

To more conclusively demonstrate that it is the premature rDNA hyper-condensation that determines a defective Cdc14 early anaphase release in *hit1*Δ and *rsa1*Δ cells, we took advantage of the capacity of rapamycin to induce nucleolar compaction [47] without affecting rDNA copy number (Figure S7A). Remarkably, rapamycin treatment severely impacted the viability of *lte1*Δ cells (Figure 7A), similar to what was shown for *hit1*Δ and *rsa1*Δ (Figures 1A and 1B). Furthermore, and also analogously to the synthetic lethality caused by simultaneous deletion of *LTE1* and either *HIT1* or *RSA1*, increased sensitivity of *lte1*Δ cells to rapamycin was rescued by the additional deletion of *BFA1* (Figure 7A). Finally, rapamycin treatment strongly compromised the viability of *tem1-3* cells, while it improved the growth of *cdc14-1* cells, as also shown for *hit1*Δ and *rsa1*Δ (Figure 7A).

Nucleolar compaction is also promoted during nutrient starvation [50], which leads to Pol I delocalization from the nucleolus and inhibition of rDNA transcription [50]. To further strengthen our results, we analyzed Cdc14 localization in cells starved of carbon or nitrogen. Remarkably, Cdc14 release was drastically reduced under these conditions, similarly as after rapamycin treatment (Figures 7B and 7C).

Since both rapamycin and starvation recapitulated the phenotypes associated with the defects in the early release of Cdc14 caused by the lack of Hit1-Rsa1, we verified whether the increased association of condensin to the rDNA in *hit1*Δ and *rsa1*Δ cells could be due to a reduction in the transcriptional activity of RNA Pol I in these mutants. Excitingly, *HIT1* or *RSA1* deletion determined a significant reduction in rRNA transcription throughout the cell cycle (Figure 7D). Therefore, our results demonstrate that defective Hit1-Rsa1 function interferes with Pol I-dependent rRNA transcription, thereby promoting rDNA hyper-condensation, which, in turn, obstructs nucleolar Cdc14 release.

DISCUSSION

Hit1 plays an important role during ribosome biogenesis in *Saccharomyces cerevisiae* [25]. Together with Rsa1, Hit1 promotes the stability of C/D box snoRNAs and facilitates normal kinetics of pre-rRNA maturation [25]. Interestingly, lack of Hit1 or Rsa1 leads to synthetic lethality in combination with loss of the MEN activator Lte1, a feature shared by mutants in which the early anaphase release of Cdc14 is compromised [24]. Here we demonstrate that the Hit1-Rsa1 snoRNP assembly factor is necessary to promote an efficient nucleolar release of Cdc14 and, thus, to ensure the proper function of this phosphatase, which establishes a fascinating new link between rRNA-associated factors and the regulation of mitotic exit. Furthermore, and excitingly, our observations demonstrate that the late condensation of the rDNA in budding yeast is necessary to efficiently coordinate mitotic exit with nucleolar segregation.

We have demonstrated that a lack of Hit1-Rsa1 facilitates condensin accessibility to the rDNA and determines nucleolar hyper-condensation. This is in agreement with previous observations suggesting that mice C/D snoRNP components p55 and p50, as well as the p50 yeast ortholog (Rvb2), could coordinate snoRNP assembly with chromatin remodeling [51, 52]. Interestingly, Rsa1/NUFIP1 interacts with Rvb1/p55 and Rvb2/p50 in both yeast and human cells, and it facilitates their recruitment on pre-snoRNPs [6, 7]. How can problems in snoRNP assembly and rRNA maturation promote nucleolar hyper-condensation? In *S. cerevisiae*, rDNA condensation only

Figure 5. Nucleolar Hyper-condensation in *hit1*Δ Cells Is Relieved by the Introduction of *ycs4-2*

(A–H) Cells expressing Spc42-mCherry and Net1-EGFP (F2301, F2303, F3388, and F3390) were grown at 23°C in YPD with 300 μg/mL adenine, arrested in G1 with 5 μg/mL α-factor, and released at 30°C into fresh medium without pheromone. (A, C, E, and G) Cell cycle progression was determined based on spindle and nuclear morphologies. Percentages of metaphase and anaphase cells are shown. Error bars represent SD (n = 3). (B, D, F, and H) Percentage of cells within each of the pre-established categories of nucleolar compaction is shown. Error bars represent SD (n = 3).

(I) Cells (F496, F2000, F2613, F2767, F2810, and F3408) were plated by spotting 10-fold serial dilutions of a culture (OD_{600} = 0.5) on YPD and incubated at the indicated temperatures.

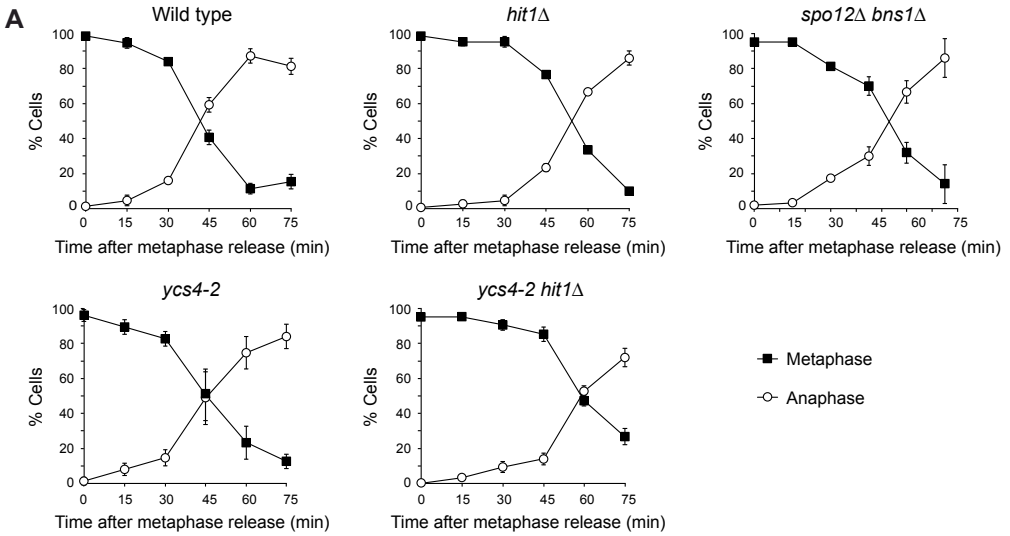

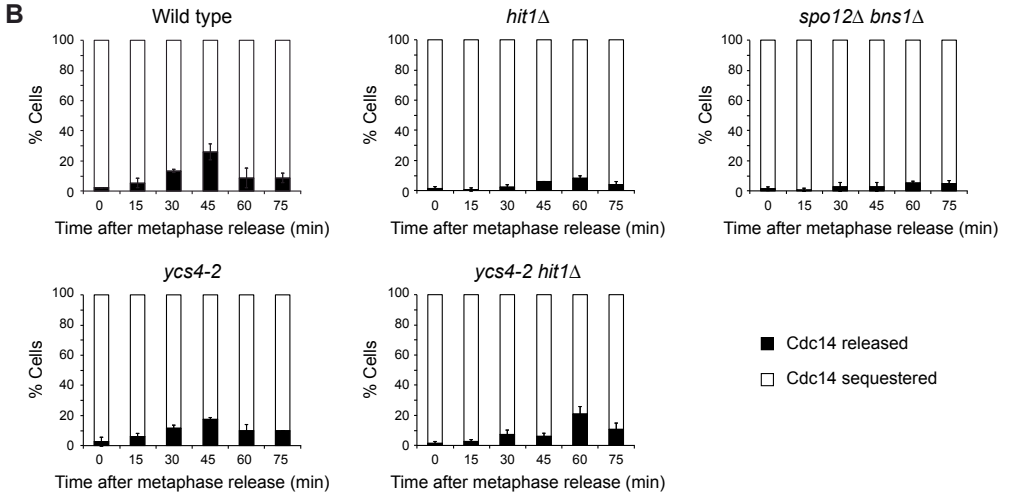

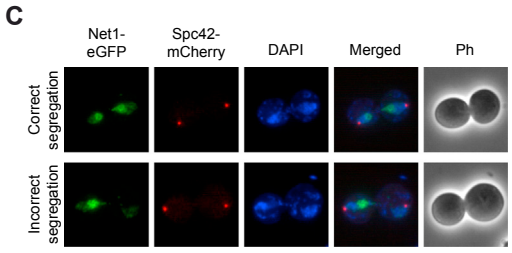

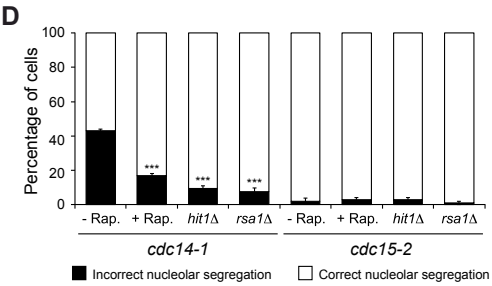

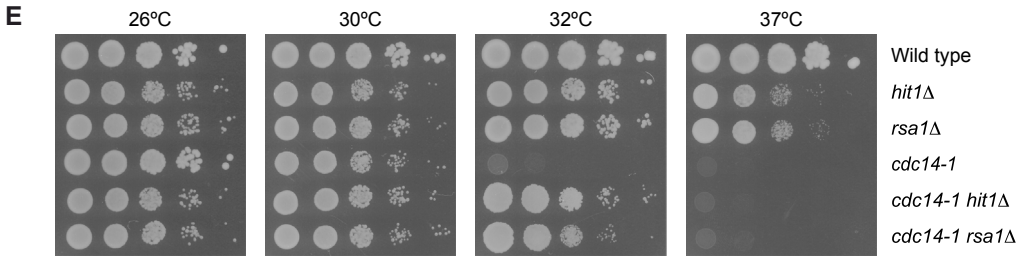

(legend on next page)

occurs once rRNA transcription is significantly reduced by the Cdc14-dependent inhibition of RNA Pol I during anaphase [14, 15, 17]. Remarkably, our results demonstrate that *HIT1* or *RSA1* deletion impairs Pol I activity, thus facilitating condensin loading on the rDNA. Despite that pre-rRNA processing and modification were initially proposed to take place on the completed transcript, it has been later shown that these processes occur co-transcriptionally and that they are, in fact, coordinated [53, 54]. As such, the SSU processome, a large complex required for small ribosomal subunit biogenesis, is also essential to ensure an efficient Pol I transcription, although the mechanism by which it links both processes remains unknown [54]. Remarkably, Hit1-Rsa1 play a key role in the early assembly of the U3 snoRNP, an essential component of the SSU processome [54, 55]. Thus, a lack of Hit1-Rsa1 could interfere with the function of the SSU processome in promoting Pol I transcription. However, besides interfering with rRNA transcription, we do not exclude that defects in snoRNP assembly could also promote nucleolar compaction by additional means. As such, snoRNPs could facilitate recruitment of specific decondensation factors to the rDNA. Interestingly, the analysis of chromatin-associated RNAs (caRNAs) in *Drosophila* cells indicated a strong enrichment in snoRNA molecules, which stably interact with chromatin and recruit the decondensation factor Df31 at specific chromatin domains to maintain them in an accessible state [56]. This enrichment was also observed in human cells, suggesting an evolutionarily conserved process. Hence, our results could provide further support to an emerging body of evidences favoring an essential role of snoRNAs and snoRNA-associated proteins in modulating the accessibility of chromatin regions and the proper establishment of the nuclear and nucleolar architecture.

Interestingly, increased rDNA compaction in *hit1*Δ and *rsa1*Δ cells impairs the function of the FEAR pathway and the timely nucleolar release of Cdc14. Accordingly, defects in the early anaphase liberation of the phosphatase caused by a lack of Hit1-Rsa1 can be alleviated by reducing condensin activity using a temperature-sensitive mutant of the condensin subunit Ycs4. Also supporting this idea, the problems associated with the defective Cdc14 release in *hit1*Δ and *rsa1*Δ cells can be recapitulated by promoting rDNA hyper-condensation using rapamycin or starving cells of nutrients. The nucleolar retention of Cdc14 during starvation is fascinating, and it suggests that sequestration of this phosphatase by means of an increased nucleolar condensation could be used as a strategy to restrict cell cycle progression under certain physiological conditions. It would be interesting to further analyze in the future whether this is the case and the factors that contribute to Cdc14 retention under these conditions.

Due to the defects in the initial nucleolar release of Cdc14, the *hit1*Δ and *rsa1*Δ mutants become highly dependent on the MEN-activating function of Lte1 to finally promote liberation of the phosphatase and mitotic exit, which explains the synthetic lethality caused by simultaneous deletion of *LTE1* and *HIT1* or *RSA1*. This phenotype could be further enhanced by the fact that *lte1*Δ selectively delays the release of Brn1 from the rDNA, which has a negative impact in nucleolar decompaction in late anaphase [57]. Nucleolar hyper-condensation could affect Cdc14 release by impeding the destabilization of its binding to Cfi1/Net1. Accordingly, expression of a Cdc14 mutant protein with reduced affinity to its inhibitor [40] efficiently rescues *hit1*Δ and *lte1*Δ synthetic lethality. Although a lack of Hit1-Rsa1 does not seem to interfere with Cdc14 or Cfi1/Net1 phosphorylation by the Polo-like kinase Cdc5, which promotes nucleolar release of the phosphatase [42], we cannot exclude that increased association of Cdc14 and Cfi1/Net1 in *hit1*Δ and *rsa1*Δ cells was caused by reduced accessibility of these proteins for Cdc5. Alternatively, increased rDNA compaction could simply impose a physical constraint to the release of Cdc14.

A defective FEAR-dependent Cdc14 liberation impairs rDNA condensation and nucleolar segregation [14, 15]. Remarkably, our results further demonstrate now that, contrariwise, premature rDNA condensation impairs FEAR function and timely Cdc14 release. In contrast to *spo12*Δ *bns1*Δ cells, in which defective FEAR-dependent Cdc14 liberation interferes with the dynamics of rDNA condensation, in *hit1*Δ and *rsa1*Δ cells it is the release of the phosphatase that is affected by alterations in the process of rDNA compaction. This differential behavior allowed us to finally provide an explanation to a long-standing open question. rDNA segregation in budding yeast encompasses two temporally separated steps: a first step comprising the unzipping of the rDNA locus from its most centromere-proximal to its most centromere-distal region, and a second step that involves rDNA compaction and depends on Cdc14 [44]. This Cdc14-dependent condensation of the rDNA only occurs during anaphase and is independent of cohesion [14, 15, 43, 44]. Intriguingly, the reason for the maintenance of a cohesin-independent linkage at the rDNA until anaphase onset is still unknown. Our results now provide a definitive answer to this conundrum. Since Cdc14 activity is mainly regulated by means of its subcellular localization, the precise control of its nucleolar release is of pivotal importance for the cells in order to temporally

Figure 6. Reducing Condensin Activity Alleviates Defective Cdc14 Release in *hit1*Δ Cells

(A and B) Cells carrying *cdc15-as1*, *pMET3-CDC20*, and *3HA-CDC14* alleles (F2073, F2205, F2508, F2880, and F2884) were blocked in metaphase (t = 0 min), as in Figures 3C–3J but at 30°C. Subsequently, cells were released into minimal medium without methionine, with 10 μM 1-NA-PP1, and at 30°C. (A) Cell cycle progression was determined based on spindle and nuclear morphologies. Percentages of metaphase and anaphase cells are shown. Error bars represent SD (n = 3). (B) Percentage of cells displaying 3HA-Cdc14 sequestered (white bars) or released (black bars) from the nucleolus is shown. Error bars represent SD (n = 3).

(C and D) *cdc14-1* (F3318, F3443, and F3444) and *cdc15-2* (F3449, F3450, and F3451) cells expressing Net1-EGFP and Spc42-mCherry were arrested in anaphase at 34°C for 2.5 hr. (C) Representative images display correct and incorrect nucleolar segregation. Nuclear (DAPI, blue) and nucleolar (Net1-EGFP, green) morphologies, the SPBs (Spc42-mCherry, red), a Ph, and a merged image are shown. (D) Percentage of cells displaying correct (white bars) or incorrect (black bars) nucleolar segregation is shown. As a control, cells were treated (+Rap) or not (−Rap) with 20 nM rapamycin. Error bars represent SD (n = 3). Statistically significant differences (***p < 0.001) relative to the untreated control (−Rap), and according to a one-way ANOVA test, are also shown.

(E) Cells (F496, F2000, F2613, F3311, F3445, and F3446) were plated, by spotting 10-fold serial dilutions of a culture (OD_{600} = 0.5) on YPD, and incubated at the indicated temperatures.

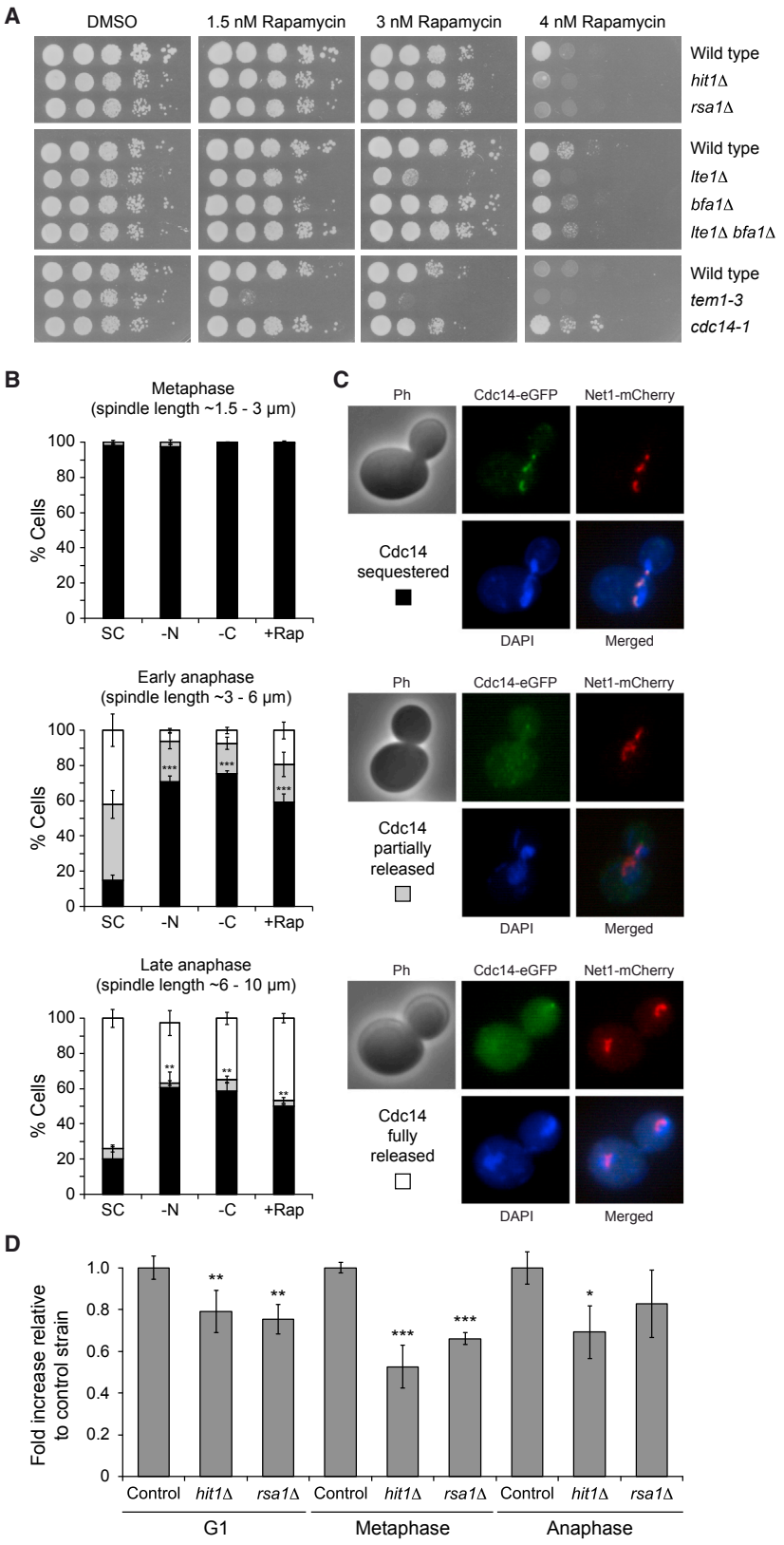

Figure 7. rDNA Transcription Is Reduced in the Absence of Hit1-Rsa1

(A) Ten-fold serial dilutions from cell cultures (F496, F2000, F2613, F549, F533, F986, F2135, and F3311) at OD_{600} = 0.5 were spotted on YPD plates without (DMSO) or with 1.5, 3, or 4 nM rapamycin and incubated at 23°C. (B and C) Cells expressing Cdc14-EGFP and Net1-mCherry (F3424) and growing in minimal medium (SC) were switched to SC without nitrogen (−N), SC without carbon (−C), or treated with 20 nM rapamycin (+Rap) for 1 hr. (B) Graph represents the percentage of metaphase and early and late anaphase cells (estimated by spindle length) with Cdc14-EGFP sequestered (black bars) or partially (gray bars) or fully released (white bars) from the nucleolus. Error bars represent SEM (n = 3). Statistically significant differences (***$p < 0.001$ and **$p < 0.01$) in the percentage of cells with Cdc14 sequestered relative to that of cells growing in SC, and according to a one-way ANOVA test, are also shown. (C) Representative images display Cdc14-EGFP localization (green). Net1-mCherry (red), nuclear morphology (DAPI, blue), a phase-contrast (Ph) image, and a merged image are also shown.

(D) Quantification of rRNA transcription by RT-PCR, using primers for the *ITS2* region of the rDNA and for the internal reference gene *PDA1*, in *cdc15-as1* (control, F511), *hit1*Δ *cdc15-as1* (*hit1*Δ, F3334), and *rsa1*Δ *cdc15-as1* (*rsa1*Δ, F3338) cells arrested either in G1 with 5 μg/mL α-factor, in metaphase with 150 μg/mL nocodazole, or in anaphase with 10 μM 1-NA-PP1. Graph indicates fold increase relative to the *cdc15-as1* control strain (F511). Error bars indicate SEM (n = 3). Statistically significant differences (***$p < 0.001$, **$p < 0.01$, and *$p < 0.05$) relative to the control, and according to a one-way ANOVA test, are also shown.

coordinate key cell cycle events [10, 13, 14]. Chromosome condensation, which imparts longitudinal rigidity to withstand spindle forces and facilitates disentanglement of sister chromatids [58], is also a fundamental process that must be actively promoted before chromosomes are allowed to segregate. However, our results demonstrate that premature rDNA condensation imposes a problem for the proper nucleolar release of Cdc14. The easiest way to circumvent this problem is by specifically placing rDNA condensation under the control of Cdc14, so that, only when the activity of this phosphatase is promoted, cells are allowed to initiate nucleolar compaction. Therefore, the late Cdc14-dependent rDNA condensation ensures that proper segregation of this chromosomal region takes place without affecting mitotic exit signaling.

The nucleolar proteome is largely conserved throughout evolution [1, 59]. Excitingly, Hit1 shows sequence homology with ZNHIT3, a human nucleolar protein. Furthermore, and similarly to Hit1, ZNHIT3 regulates the abundance of NUFIP1, the human functional Rsa1 homolog [25]. Cdc14 is also conserved in humans, where two Cdc14 orthologs are expressed: CDC14A and CDC14B [60]. Interestingly, CDC14B localizes to the nucleolus in interphase, and it is later dispersed throughout the cell at the onset of mitosis, although there is controversy about its actual role [60, 61]. CDC14B also relocalizes from the nucleolus to the nucleus in response to genotoxic stress, which could be important for an efficient activation of the DNA damage checkpoint [62]. Hence, in light of our results, it would be interesting to analyze whether nucleolar localization of CDC14B is affected by the lack of ZNHIT3, which could help to clarify the functional role of this phosphatase.

STAR★METHODS

Detailed methods are provided in the online version of this paper and include the following:

- KEY RESOURCES TABLE
- CONTACT FOR REAGENT AND RESOURCE SHARING
- EXPERIMENTAL MODEL AND SUBJECT DETAILS
  - Yeast strains
  - Culture/growth conditions
- METHOD DETAILS
  - Plasmids
  - Visualization of fluorescently tagged proteins
  - Immunofluorescence
  - Mitotic spreads
  - Western blotting
  - FACS analysis
  - Chromatin immunoprecipitation
  - Quantification of rRNA transcription
  - Genomic DNA extraction
  - Estimation of rDNA copy number in genomic DNA
- QUANTIFICATION AND STATISTICAL ANALYSIS

SUPPLEMENTAL INFORMATION

Supplemental Information includes seven figures and five tables and can be found with this article online at https://doi.org/10.1016/j.cub.2017.09.028.

AUTHORS CONTRIBUTIONS

F.M.-C., A.I.d.l.S.-V., I.G.d.O., and J.M.-L. designed the experiments. A.I.d.l.S.-V., I.G.d.O., and J.M.-L. carried out the experiments. F.M.-C., A.I.d.l.S.-V., I.G.d.O., and J.M.-L. analyzed the data. F.M.-C. wrote the manuscript.

ACKNOWLEDGMENTS

We thank Félix Prado and members of the Monje-Casas lab for critical reading of the manuscript, José Carlos Blanco for technical support, and Jesús de la Cruz for helpful comments. We also thank Félix Prado and Simonetta Piatti for generous gifts of strains. This work was supported by the Andalusian Regional Government, the European Regional Development Fund (FEDER), and the Spanish Ministry of Economy and Competitiveness (BFU2013-43718-P and BFU2016-76642-P).

Received: May 19, 2017
Revised: August 16, 2017
Accepted: September 13, 2017
Published: October 19, 2017

REFERENCES

1. Boisvert, F.M., van Koningsbruggen, S., Navascués, J., and Lamond, A.I. (2007). The multifunctional nucleolus. Nat. Rev. Mol. Cell Biol. *8*, 574–585.
2. Woolford, J.L., Jr., and Baserga, S.J. (2013). Ribosome biogenesis in the yeast Saccharomyces cerevisiae. Genetics *195*, 643–681.
3. Bratkovič, T., and Rogelj, B. (2014). The many faces of small nucleolar RNAs. Biochim. Biophys. Acta *1839*, 438–443.
4. Dupuis-Sandoval, F., Poirier, M., and Scott, M.S. (2015). The emerging landscape of small nucleolar RNAs in cell biology. Wiley Interdiscip. Rev. RNA *6*, 381–397.
5. Lafontaine, D.L. (2015). Noncoding RNAs in eukaryotic ribosome biogenesis and function. Nat. Struct. Mol. Biol. *22*, 11–19.
6. Boulon, S., Marmier-Gourrier, N., Pradet-Balade, B., Wurth, L., Verheggen, C., Jády, B.E., Rothé, B., Pescia, C., Robert, M.C., Kiss, T., et al. (2008). The Hsp90 chaperone controls the biogenesis of L7Ae RNPs through conserved machinery. J. Cell Biol. *180*, 579–595.
7. McKeegan, K.S., Debieux, C.M., and Watkins, N.J. (2009). Evidence that the AAA+ proteins TIP48 and TIP49 bridge interactions between 15.5K and the related NOP56 and NOP58 proteins during box C/D snoRNP biogenesis. Mol. Cell. Biol. *29*, 4971–4981.
8. Visintin, R., and Amon, A. (2000). The nucleolus: the magician's hat for cell cycle tricks. Curr. Opin. Cell Biol. *12*, 372–377.
9. Audas, T.E., Jacob, M.D., and Lee, S. (2012). The nucleolar detention pathway: A cellular strategy for regulating molecular networks. Cell Cycle *11*, 2059–2062.
10. Stegmeier, F., and Amon, A. (2004). Closing mitosis: the functions of the Cdc14 phosphatase and its regulation. Annu. Rev. Genet. *38*, 203–232.
11. Shou, W., Seol, J.H., Shevchenko, A., Baskerville, C., Moazed, D., Chen, Z.W., Jang, J., Shevchenko, A., Charbonneau, H., and Deshaies, R.J. (1999). Exit from mitosis is triggered by Tem1-dependent release of the protein phosphatase Cdc14 from nucleolar RENT complex. Cell *97*, 233–244.
12. Visintin, R., Hwang, E.S., and Amon, A. (1999). Cfi1 prevents premature exit from mitosis by anchoring Cdc14 phosphatase in the nucleolus. Nature *398*, 818–823.
13. Rock, J.M., and Amon, A. (2009). The FEAR network. Curr. Biol. *19*, R1063–R1068.
14. D'Amours, D., Stegmeier, F., and Amon, A. (2004). Cdc14 and condensin control the dissolution of cohesin-independent chromosome linkages at repeated DNA. Cell *117*, 455–469.

15. Sullivan, M., Higuchi, T., Katis, V.L., and Uhlmann, F. (2004). Cdc14 phosphatase induces rDNA condensation and resolves cohesin-independent cohesion during budding yeast anaphase. Cell *117*, 471–482.
16. Torres-Rosell, J., Machín, F., Jarmuz, A., and Aragón, L. (2004). Nucleolar segregation lags behind the rest of the genome and requires Cdc14p activation by the FEAR network. Cell Cycle *3*, 496–502.
17. Clemente-Blanco, A., Mayán-Santos, M., Schneider, D.A., Machín, F., Jarmuz, A., Tschochner, H., and Aragón, L. (2009). Cdc14 inhibits transcription by RNA polymerase I during anaphase. Nature *458*, 219–222.
18. Shirayama, M., Matsui, Y., and Toh-E, A. (1994). The yeast TEM1 gene, which encodes a GTP-binding protein, is involved in termination of M phase. Mol. Cell. Biol. *14*, 7476–7482.
19. Bardin, A.J., Visintin, R., and Amon, A. (2000). A mechanism for coupling exit from mitosis to partitioning of the nucleus. Cell *102*, 21–31.
20. Pereira, G., Höfken, T., Grindlay, J., Manson, C., and Schiebel, E. (2000). The Bub2p spindle checkpoint links nuclear migration with mitotic exit. Mol. Cell *6*, 1–10.
21. Visintin, R., and Amon, A. (2001). Regulation of the mitotic exit protein kinases Cdc15 and Dbf2. Mol. Biol. Cell *12*, 2961–2974.
22. Lee, S.E., Frenz, L.M., Wells, N.J., Johnson, A.L., and Johnston, L.H. (2001). Order of function of the budding-yeast mitotic exit-network proteins Tem1, Cdc15, Mob1, Dbf2, and Cdc5. Curr. Biol. *11*, 784–788.
23. Grandin, N., de Almeida, A., and Charbonneau, M. (1998). The Cdc14 phosphatase is functionally associated with the Dbf2 protein kinase in Saccharomyces cerevisiae. Mol. Gen. Genet. *258*, 104–116.
24. Ye, P., Peyser, B.D., Pan, X., Boeke, J.D., Spencer, F.A., and Bader, J.S. (2005). Gene function prediction from congruent synthetic lethal interactions in yeast. Mol. Syst. Biol. *1*, 2005.0026.
25. Rothé, B., Saliou, J.M., Quinternet, M., Back, R., Tiotiu, D., Jacquemin, C., Loegler, C., Schlotter, F., Peña, V., Eckert, K., et al. (2014). Protein Hit1, a novel box C/D snoRNP assembly factor, controls cellular concentration of the scaffolding protein Rsa1 by direct interaction. Nucleic Acids Res. *42*, 10731–10747.
26. Wang, Y., Hu, F., and Elledge, S.J. (2000). The Bfa1/Bub2 GAP complex comprises a universal checkpoint required to prevent mitotic exit. Curr. Biol. *10*, 1379–1382.
27. Stegmeier, F., Huang, J., Rahal, R., Zmolik, J., Moazed, D., and Amon, A. (2004). The replication fork block protein Fob1 functions as a negative regulator of the FEAR network. Curr. Biol. *14*, 467–480.
28. Boeke, J.D., Trueheart, J., Natsoulis, G., and Fink, G.R. (1987). 5-Fluoroorotic acid as a selective agent in yeast molecular genetics. Methods Enzymol. *154*, 164–175.
29. Caydasi, A.K., Khmelinskii, A., Duenas-Sanchez, R., Kurtulmus, B., Knop, M., and Pereira, G. (2017). Temporal and compartment-specific signals coordinate mitotic exit with spindle position. Nat. Commun. *8*, 14129.
30. Cohen-Fix, O., Peters, J.M., Kirschner, M.W., and Koshland, D. (1996). Anaphase initiation in Saccharomyces cerevisiae is controlled by the APC-dependent degradation of the anaphase inhibitor Pds1p. Genes Dev. *10*, 3081–3093.
31. Wäsch, R., and Cross, F.R. (2002). APC-dependent proteolysis of the mitotic cyclin Clb2 is essential for mitotic exit. Nature *418*, 556–562.
32. Kawakami, K., Shafer, B.K., Garfinkel, D.J., Strathern, J.N., and Nakamura, Y. (1992). Ty element-induced temperature-sensitive mutations of Saccharomyces cerevisiae. Genetics *131*, 821–832.
33. Reijo, R.A., Cho, D.S., and Huffaker, T.C. (1993). Deletion of a single-copy tRNA affects microtubule function in Saccharomyces cerevisiae. Genetics *135*, 955–962.
34. Wickner, R.B., Koh, T.J., Crowley, J.C., O'Neil, J., and Kaback, D.B. (1987). Molecular cloning of chromosome I DNA from Saccharomyces cerevisiae: isolation of the MAK16 gene and analysis of an adjacent gene essential for growth at low temperatures. Yeast *3*, 51–57.
35. Kressler, D., Doère, M., Rojo, M., and Linder, P. (1999). Synthetic lethality with conditional dbp6 alleles identifies rsa1p, a nucleoplasmic protein involved in the assembly of 60S ribosomal subunits. Mol. Cell. Biol. *19*, 8633–8645.
36. Rothé, B., Back, R., Quinternet, M., Bizarro, J., Robert, M.C., Blaud, M., Romier, C., Manival, X., Charpentier, B., Bertrand, E., and Branlant, C. (2014). Characterization of the interaction between protein Snu13p/15.5K and the Rsa1p/NUFIP factor and demonstration of its functional importance for snoRNP assembly. Nucleic Acids Res. *42*, 2015–2036.
37. Bishop, A.C., Ubersax, J.A., Petsch, D.T., Matheos, D.P., Gray, N.S., Blethrow, J., Shimizu, E., Tsien, J.Z., Schultz, P.G., Rose, M.D., et al. (2000). A chemical switch for inhibitor-sensitive alleles of any protein kinase. Nature *407*, 395–401.
38. Stegmeier, F., Visintin, R., and Amon, A. (2002). Separase, polo kinase, the kinetochore protein Slk19, and Spo12 function in a network that controls Cdc14 localization during early anaphase. Cell *108*, 207–220.
39. Holt, L.J., Krutchinsky, A.N., and Morgan, D.O. (2008). Positive feedback sharpens the anaphase switch. Nature *454*, 353–357.
40. Shou, W., Sakamoto, K.M., Keener, J., Morimoto, K.W., Traverso, E.E., Azzam, R., Hoppe, G.J., Feldman, R.M., DeModena, J., Moazed, D., et al. (2001). Net1 stimulates RNA polymerase I transcription and regulates nucleolar structure independently of controlling mitotic exit. Mol. Cell *8*, 45–55.
41. Sung, M.K., and Huh, W.K. (2007). Bimolecular fluorescence complementation analysis system for in vivo detection of protein-protein interaction in Saccharomyces cerevisiae. Yeast *24*, 767–775.
42. Visintin, R., Stegmeier, F., and Amon, A. (2003). The role of the polo kinase Cdc5 in controlling Cdc14 localization. Mol. Biol. Cell *14*, 4486–4498.
43. Lavoie, B.D., Hogan, E., and Koshland, D. (2004). In vivo requirements for rDNA chromosome condensation reveal two cell-cycle-regulated pathways for mitotic chromosome folding. Genes Dev. *18*, 76–87.
44. Machín, F., Torres-Rosell, J., Jarmuz, A., and Aragón, L. (2005). Spindle-independent condensation-mediated segregation of yeast ribosomal DNA in late anaphase. J. Cell Biol. *168*, 209–219.
45. Lopez-Serra, L., Lengronne, A., Borges, V., Kelly, G., and Uhlmann, F. (2013). Budding yeast Wapl controls sister chromatid cohesion maintenance and chromosome condensation. Curr. Biol. *23*, 64–69.
46. Geil, C., Schwab, M., and Seufert, W. (2008). A nucleolus-localized activator of Cdc14 phosphatase supports rDNA segregation in yeast mitosis. Curr. Biol. *18*, 1001–1005.
47. Wang, B.D., Butylin, P., and Strunnikov, A. (2006). Condensin function in mitotic nucleolar segregation is regulated by rDNA transcription. Cell Cycle *5*, 2260–2267.
48. Lavoie, B.D., Hogan, E., and Koshland, D. (2002). In vivo dissection of the chromosome condensation machinery: reversibility of condensation distinguishes contributions of condensin and cohesin. J. Cell Biol. *156*, 805–815.
49. Wang, D., Mansisidor, A., Prabhakar, G., and Hochwagen, A. (2016). Condensin and Hmo1 Mediate a Starvation-Induced Transcriptional Position Effect within the Ribosomal DNA Array. Cell Rep. *14*, 1010–1017.
50. Tsang, C.K., Li, H., and Zheng, X.S. (2007). Nutrient starvation promotes condensin loading to maintain rDNA stability. EMBO J. *26*, 448–458.
51. King, T.H., Decatur, W.A., Bertrand, E., Maxwell, E.S., and Fournier, M.J. (2001). A well-connected and conserved nucleoplasmic helicase is required for production of box C/D and H/ACA snoRNAs and localization of snoRNP proteins. Mol. Cell. Biol. *21*, 7731–7746.
52. Newman, D.R., Kuhn, J.F., Shanab, G.M., and Maxwell, E.S. (2000). Box C/D snoRNA-associated proteins: two pairs of evolutionarily ancient proteins and possible links to replication and transcription. RNA *6*, 861–879.
53. Kos, M., and Tollervey, D. (2010). Yeast pre-rRNA processing and modification occur cotranscriptionally. Mol. Cell *37*, 809–820.
54. Gallagher, J.E., Dunbar, D.A., Granneman, S., Mitchell, B.M., Osheim, Y., Beyer, A.L., and Baserga, S.J. (2004). RNA polymerase I transcription and pre-rRNA processing are linked by specific SSU processome components. Genes Dev. *18*, 2506–2517.

55. Rothé, B., Manival, X., Rolland, N., Charron, C., Senty-Ségault, V., Branlant, C., and Charpentier, B. (2017). Implication of the box C/D snoRNP assembly factor Rsa1p in U3 snoRNP assembly. Nucleic Acids Res. *45*, 7455–7473.

56. Schubert, T., Pusch, M.C., Diermeier, S., Benes, V., Kremmer, E., Imhof, A., and Längst, G. (2012). Df31 protein and snoRNAs maintain accessible higher-order structures of chromatin. Mol. Cell *48*, 434–444.

57. Varela, E., Shimada, K., Laroche, T., Leroy, D., and Gasser, S.M. (2009). Lte1, Cdc14 and MEN-controlled Cdk inactivation in yeast coordinate rDNA decompaction with late telophase progression. EMBO J. *28*, 1562–1575.

58. Thadani, R., and Uhlmann, F. (2015). Chromosome condensation: weaving an untangled web. Curr. Biol. *25*, R663–R666.

59. Andersen, J.S., Lyon, C.E., Fox, A.H., Leung, A.K., Lam, Y.W., Steen, H., Mann, M., and Lamond, A.I. (2002). Directed proteomic analysis of the human nucleolus. Curr. Biol. *12*, 1–11.

60. Mocciaro, A., and Schiebel, E. (2010). Cdc14: a highly conserved family of phosphatases with non-conserved functions? J. Cell Sci. *123*, 2867–2876.

61. Mailand, N., Lukas, C., Kaiser, B.K., Jackson, P.K., Bartek, J., and Lukas, J. (2002). Deregulated human Cdc14A phosphatase disrupts centrosome separation and chromosome segregation. Nat. Cell Biol. *4*, 317–322.

62. Bassermann, F., Frescas, D., Guardavaccaro, D., Busino, L., Peschiaroli, A., and Pagano, M. (2008). The Cdc14B-Cdh1-Plk1 axis controls the G2 DNA-damage-response checkpoint. Cell *134*, 256–267.

63. Longtine, M.S., McKenzie, A., 3rd, Demarini, D.J., Shah, N.G., Wach, A., Brachat, A., Philippsen, P., and Pringle, J.R. (1998). Additional modules for versatile and economical PCR-based gene deletion and modification in Saccharomyces cerevisiae. Yeast *14*, 953–961.

64. Sheff, M.A., and Thorn, K.S. (2004). Optimized cassettes for fluorescent protein tagging in Saccharomyces cerevisiae. Yeast *21*, 661–670.

65. Sikorski, R.S., and Hieter, P. (1989). A system of shuttle vectors and yeast host strains designed for efficient manipulation of DNA in Saccharomyces cerevisiae. Genetics *122*, 19–27.

66. Muñoz-Barrera, M., and Monje-Casas, F. (2014). Increased Aurora B activity causes continuous disruption of kinetochore-microtubule attachments and spindle instability. Proc. Natl. Acad. Sci. USA *111*, E3996–E4005.

67. Valerio-Santiago, M., and Monje-Casas, F. (2011). Tem1 localization to the spindle pole bodies is essential for mitotic exit and impairs spindle checkpoint function. J. Cell Biol. *192*, 599–614.

68. D'Aquino, K.E., Monje-Casas, F., Paulson, J., Reiser, V., Charles, G.M., Lai, L., Shokat, K.M., and Amon, A. (2005). The protein kinase Kin4 inhibits exit from mitosis in response to spindle position defects. Mol. Cell *19*, 223–234.

69. Murillo-Pineda, M., Cabello-Lobato, M.J., Clemente-Ruiz, M., Monje-Casas, F., and Prado, F. (2014). Defective histone supply causes condensin-dependent chromatin alterations, SAC activation and chromosome decatenation impairment. Nucleic Acids Res. *42*, 12469–12482.

70. Cuylen, S., Metz, J., and Haering, C.H. (2011). Condensin structures chromosomal DNA through topological links. Nat. Struct. Mol. Biol. *18*, 894–901.

71. Huang, J., Brito, I.L., Villén, J., Gygi, S.P., Amon, A., and Moazed, D. (2006). Inhibition of homologous recombination by a cohesin-associated clamp complex recruited to the rDNA recombination enhancer. Genes Dev. *20*, 2887–2901.

STAR★METHODS

KEY RESOURCES TABLE

REAGENT or RESOURCE	SOURCE	IDENTIFIER
Antibodies		
Anti-HA (HA.11) mouse monoclonal	Covance	Cat# MMS-101R; RRID: AB_291262
Anti-Myc rabbit polyclonal	Gramsh Laboratories	not commercially available at present
Anti-Myc (9E10) mouse monoclonal	Covance	Cat# MMS-150R; RRID: AB_291325
Anti-GFP Living Colors® (JL8) mouse monoclonal	Clontech	Cat# 632380; RRID: AB_10013427
Anti-β-actin rabbit polyclonal	Abcam	Cat# ab8227; RRID: AB_2305186
Anti-Clb2 (y-180) rabbit polyclonal	Santa Cruz Biotechnology	Cat# sc-9071; RRID: AB_667962
Anti-Nop1 (28F2) mouse monoclonal	Santa Cruz Biotechnology	Cat# sc-57940; RRID: AB_630044
Anti-Pgk1 mouse monoclonal	Invitrogen	Cat# 459250; RRID: AB_2532235
Anti-Sic1 (FL-284) rabbit polyclonal	Santa Cruz Biotechnology	Cat# sc-50441; RRID: AB_785671
Anti-tubulin (YOL1/34) rat monoclonal	Abcam	Cat# ab6161; RRID: AB_305329
Anti-mouse IgG Cy3-conjugated donkey polyclonal	Jackson ImmunoResearch	Cat# 715-165-151; RRID: AB_2315777
Anti-rabbit IgG FITC-AffiniPure goat polyclonal	Jackson ImmunoResearch	Cat# 111-095-144; RRID: AB_2337978
Anti-rat IgG FITC FITC-AffiniPure donkey polyclonal	Jackson ImmunoResearch	Cat# 712-095-153; RRID: AB_2340652
Anti-mouse IgG HRP-linked sheep polyclonal	GE Healthcare	Cat# NA931; RRID: AB_772210
Anti-rabbit IgG HRP-linked donkey polyclonal	GE Healthcare	Cat# NA934; RRID: AB_772206
Anti-V5-tag (Anti-Pk-tag) mouse monoclonal	Bio-Rad	Cat# MCA1360GA; RRID: AB_567249
Chemicals, Peptides, and Recombinant Proteins		
Yeast extract	Conda	Cat# 1702.05
Bacteriological peptone	Conda	Cat# 1616.00
D-(+)-Glucose (Dextrose)	VWR	Cat# 24379.363
D-(+)-Raffinose pentahydrate	Sigma	Cat# R0250
D-(+)-Galactose	Sigma	Cat# G0750
Yeast nitrogen base (YNB)	Becton Dickinson	Cat# 233520
L-Adenine hemisulfate salt	Sigma	Cat# A9126
L-Alanine	Sigma	Cat# A7469
L-Arginine	Sigma	Cat# A5006
L-Asparagine	Sigma	Cat# A0884
L-Aspartic Acid potassium salt	Sigma	Cat# A6558
L-Cysteine	Sigma	Cat# C7352
L-Glutamic acid monosodium salt hydrate	Sigma	Cat# G5889
L-Glutamine	Sigma	Cat# G3126
L-Histidine	Sigma	Cat# H8000
myo-Inositol	Sigma	Cat# I7508
L-Isoleucine	Sigma	Cat# I2752
L-Leucine	Sigma	Cat# L8000
L-Lysine monohydrochloride	Sigma	Cat# L5526
L-Methionine	Sigma	Cat# M9625
L-Phenylalanine	Sigma	Cat# P2126
L-Proline	Sigma	Cat# P0380
L-Serine	Sigma	Cat# S4500
L-Threonine	Sigma	Cat# T8625
L-Tryptophan	Sigma	Cat# T0254
L-Tyrosine	Sigma	Cat# T3754
Uracil	Sigma	Cat# U0750

(*Continued on next page*)

Continued

REAGENT or RESOURCE	SOURCE	IDENTIFIER
L-Valine	Sigma	Cat# V0500
Formaldehyde solution min, 37%	Merck	Cat# 1.04003.1000
Di-Potassium hydrogen phosphate (K_2HPO_4)	Merck	Cat# 1.05101.1000
Potassium dihydrogen phosphate (KH_2PO_4)	Merck	Cat# 1.04877.1000
4′,6-Diamidino-2-phenylindole dihydrochloride (DAPI)	Sigma	Cat# 32670
Citric acid	Sigma	Cat# C0759
D-Sorbitol	Sigma	Cat# S1876
Zymoliase 100T	US Biological	Cat# 37340-57-1
Glusulase	Perkin Elmer	Cat# NEE154001EA
Potassium Acetate	VWR Chemicals	Cat# 26667.236
DL-Dithiothreitol (DTT)	Sigma-Aldrich	Cat# D0632
Zymoliase 20T	US Biological	Cat# C10091454
2-(N-morpholino) ethane sulfonic acid (MES hydrate)	Sigma-Aldrich	Cat# M8250
Ethylenediamine-tetraacetic acid disodium salt dehydrate (EDTA)	Sigma	Cat# E5134
Magnesium chloride hexahydrate ($MgCl_2$)	Sigma-Aldrich	Cat# M0250
Photoflo	Sigma	Cat# P6148
Bovine serum albumin (BSA)	Sigma	Cat# A4503
Gelatine	VWR	Cat# 24360.233
Vectashield mounting media (without DAPI)	Vector Laboratories	Cat# H-1000
Sodium chloride (NaCl)	Merck	Cat# 7647-14-5
Potassium chloride (KCl)	Merck	Cat# 1.04963.1000
Tricloroacetic acid (TCA)	Merck	Cat# 1.00807.1000
Trizma® Base	Sigma	Cat# T1503
Complete EDTA-free protease inhibitor cocktail	Roche	Cat# 11873580001
Glass-Beads	Sigma	Cat# G9268
Acetone	Merck	Cat# 1.00014.1000
2-Mercaptoethanol	Sigma	Cat# M6250
Glycerol	Sigma	Cat# G7893
Bromophenol Blue	Sigma-Aldrich	Cat# B0126
37.5:1 Acrylamide:bisacrylamide solution (Protogel)	National Diagnostics	Cat# EC-890
Nitrocellulose Blotting Membrane 0,45 μm	GE Healthcare	Cat# 10600008
Western Bright™ ECL	Advansta	Cat# K-12045-D20
RNase A	Sigma	Cat# R4875
Ethanol 100%	Emsure	Cat# 1.00983.2511
Propidium iodide	Sigma	Cat# P4170
Glycine	Sigma	Cat# G7126
4-(2-Hydroxyethyl) piperazine-1-ethanesulfonic acid (HEPES)	Sigma	Cat# H4034
Potassium hydroxide (KOH)	Merck	Cat# 1.05033.1000
Triton X-100	Merck	Cat# 1.08603.1000
Sodium deoxycholate	Sigma	Cat# D6750
Phenylmethanesulfonyl fluoride (PMSF)	Sigma	Cat# P7626
A-Sepharose® CL-4B beads	GE Healthcare	Cat# GE17-0780-01
Lithium chloride (LiCl)	Sigma	Cat# L9650
Igepal CA-630	Sigma-Aldrich	Cat# I3021
Sodium dodecyl sulfate (SDS)	Sigma	Cat# 71725
Pronase (Protease from *Streptomyces griseus*)	Sigma	Cat# P6911
Glycogen type IX from bovine liver	Sigma-Aldrich	Cat# G0885
Phenol-chloroform-isoamyl-alcohol mixture	Sigma	Cat# 101246723
iTaq Universal SYBR® Green Supermix	Bio-Rad	Cat# 172-5122MP2

(*Continued on next page*)

Continued		
REAGENT or RESOURCE	SOURCE	IDENTIFIER
Phenol	VWR	Cat# 1.00206.0250
Chloroform	VWR	Cat# 22711.290
Sodium acetate trihydrate	Merck	Cat# 1.06267.1000
DNase I	Invitrogen	Cat# 18068-015
Critical Commercial Assays		
SuperScript® III First-Strand Synthesis System	Invitrogen	Cat# 18080-051
Software and Algorithms		
LAS AF Software	Leica	http://www.leica-microsystems.com
ImageJ Software	NIH	http://rsbweb.nih.gov/ij
7500 Real-Time PCR Software v2.06	Applied Biosystems	http://www.thermofisher.com
Image Lab Software v5.1, build 8	Bio-Rad Laboratories	http://www.bio-rad.com

CONTACT FOR REAGENT AND RESOURCE SHARING

In order to request strains, protocols, or any materials generated in this study, please contact the Lead Contact, Fernando Monje-Casas (fernando.monje@cabimer.es).

EXPERIMENTAL MODEL AND SUBJECT DETAILS

Yeast strains

All yeast strains are derivatives of W303, except from F3040, F3682 and F3683 (BY background), and their genotypes are described in Table S1. Strains expressing 13Myc-tagged versions of Hit1 or Rsa1, eGFP-tagged proteins, and the strains for the BiFC analyses were constructed by integrating the corresponding tag by homologous recombination using the plasmids described in [63], [64] and [41], respectively. Construction of strains carrying deletions of the *HIT1* or *RSA1* genes was carried out using the same strategy, but introducing a cassette with a selectable marker that replaced the endogenous gene, using the plasmids detailed in [63].

Culture/growth conditions

Cells were cultured in YPD (rich medium containing 1% yeast extract, 2% peptone and 2% dextrose), YPRaf (rich medium containing 1% yeast extract, 2% peptone and 2% raffinose), YPRaf/Gal (rich medium containing 1% yeast extract, 2% peptone, 2% raffinose and 2% galactose), or SC (minimal medium containing 0.67% yeast nitrogen base, 2% dextrose, 0.13% drop-out mix, 0.002% tryptophan, 0.002% histidine, 0.012% leucine, 0.002% methionine and 0.002% uracil). The drop-out mix included supplements required for strains growth, and was prepared by mixing 0.5 g adenine, 2 g alanine, 2 g arginine, 2 g asparagine, 2 g aspartic acid, 2 g cysteine, 2 g glutamine, 2 g glutamic acid, 2 g glycine, 2 g inositol, 2 g isoleucine, 2 g lysine, 2 g phenylalanine, 2 g proline, 2 g serine, 2 g threonine, 2 g tyrosine and 2 g valine. Liquid cultures were grown in flasks, maintaining a constant 1/5 culture/flask volume ratio. Plates for cell culture contained 25 mL of the previously detailed medium with 2% agar. Specific modifications in the composition of the medium, as well as the growth temperature can be found in the figure legends.

METHOD DETAILS

Plasmids

The YCp50-*LTE1* plasmid carrying the *LTE1* gene under its own promoter and the *URA3* marker was previously described in [27]. The plasmids for overexpression of Hit1, Rsa1 or Spo12 were generated by amplification of the corresponding ORF from yeast genomic DNA and its subsequent cloning under control of the *pGAL1-10* gene promoter in the pRS316 plasmid, originally described in [65]. Oligonucleotide sequences used for cloning of the genes are shown in Table S4.

Visualization of fluorescently tagged proteins

Samples for eGFP, Venus, mCherry, and DAPI imaging were prepared as described in [66]. In brief, samples were fixed for 10 min in 2.5% formaldehyde, washed twice with 0.1 M potassium phosphate buffer (pH 6.6), and resuspended in 0.1 M potassium phosphate buffer (pH 7.4). When DAPI staining was also required, cells were further fixed for 10 min in 80% (vol./vol.) ethanol and finally resuspended in 10 μg/mL DAPI. Samples were analyzed and imaged using a DM6000 microscope (Leica) equipped with a 100x/1.40 NA oil immersion objective lens, A4, L5, CFP, and TX2 filters, and a DF350 digital charge-coupled device camera (Leica). Images were processed with LAS AF (Leica) and ImageJ (http://rsbweb.nih.gov/ij/) software. ImageJ was further used to quantify the intensity of the fluorescent signal displayed by eGFP-tagged proteins in different cell compartments and to measure nucleolar area in cells expressing Net1-eGFP.

Immunofluorescence

Immunofluorescence was carried out as described in [67]. Specifically, cells were fixed in 3.7% formaldehyde and 0.1 M potassium phosphate buffer (pH 6.4) for 15 min at room temperature for nucleolar proteins or overnight at 4°C for tubulin. Cells were then washed twice with 0.1 M potassium phosphate buffer (pH 6.4), and resuspended in 1.2 M sorbitol in 0.12 M K_2HPO_4/0.033 M citric acid (pH 5.9). Fixed cells were digested with 0.1 mg/mL Zymolyase 100T (US Biological) and 1/10 volume of glusulase (Perkin Elmer) at 30°C for 15 min, washed once, and resuspended in 1.2 M sorbitol in 0.12 M K_2HPO_4/0.033 M citric acid (pH 5.9). Antibodies were used at the concentrations described in Table S2. Microscope preparations were analyzed and imaged as previously described for the visualization of fluorescently tagged proteins.

Mitotic spreads

Mitotic spreads were prepared as described in [66]. In brief, exponential cultures were grown overnight, and 2 mL of culture were centrifuged and resuspended in 200 μL of 2% potassium acetate and 1M sorbitol solution. 2 μL 1M DTT and 5 μL of Zymolyase 20T (10 mg/mL) were added, and cells were digested at 30°C from 30-60 min. The reaction was stopped by centrifugation at 4°C and 350 g, after which cells were resuspended in 1 mL of ice-cold MES-Sorbitol (0.1M 2-(*N*-morpholino) ethane sulfonic acid, 1 mM EDTA, 0.5 mM $MgCl_2$, 1 M sorbitol). Spheroplasts were collected by centrifugation at 4°C and 350 g, and softly resuspended in 200 μL of MES. Cell suspension was prefixed with 720 μL of 4% paraformaldehyde, and then placed on a clean ethanol-treated slide, spread with a coverslip, and incubated at room temperature for 30 min. Spread preparation was washed with 1 mL of 0.4% Photoflo (Sigma P6148) solution and dried at room temperature 2-12 hr. Spread sample was washed with 1 mL PBS for 10 min and then incubated with 200 μL of blocking solution (0.2% gelatine, 0.5% BSA in PBS) for 1 hr. Next, sample was first incubated for 2 hr with the primary antibody in a wet chamber at room temperature, and then for another 2 hr with the secondary antibody, both prepared in blocking solution. After each incubation, antibodies were washed three times with PBS for 5 min. Finally, one drop of VectaShield (Vector Labs) with 1 μg/mL DAPI was added, and spread with a coverslip. Antibodies were used at the concentrations described in Table S2. Microscope preparations were analyzed and imaged as previously described for the visualization of fluorescently tagged proteins.

Western blotting

Protein extracts were prepared using the trichloroacetic acid (TCA) precipitation method detailed in [68]. Specifically, cells from 10 mL of a liquid culture were incubated for 10 min in 5% TCA. Samples were centrifuged for 3 min at maximum speed and 4°C. Pellets were transferred to a clean microcentrifuge tube, centrifuged again to wash out residual TCA, and resupended by vortex in 1 mL of acetone at room temperature. Once resuspended, the sample was centrifuged again for 6 min at maximum speed, and the collected pellets were completely dried in a hood. Cells were resuspended in 100 μL of lysis buffer (50 mM Tris-HCl (pH 7.5), 1 mM EDTA, 50 mM DTT, 1 mM PMSF, and complete EDTA-free protease inhibitor cocktail (Roche)). After adding an equal volume of glass beads, cells were broken in a multivortex for 40 min. Finally, 1x sample buffer was added, and the protein extract was boiled before loading in a polyacrylamide gel. Electrophoresis was carried out using a SE600 Hoefer electrophoresis system or a Mini-Protean System (Bio-Rad), and proteins were transferred to a 0.45 μm nitrocellulose membrane (GE Healthcare) using a TE62 tank transfer unit (Amersham) or a Mini-Protean transfer system (Bio-Rad). Antibodies were used at the concentrations described in Table S3. Protein signal was detected using the Western Bright ECL system (Advansta). Western blot images were acquired either exposing Amersham Hyperfilm™ chemiluminescence films (GE Healthcare) or using the Chemidoc™ MP system with the Image Lab software (Bio-Rad).

FACS analysis

FACS analysis was performed as detailed in [66]. Briefly, cells were fixed in 70% (vol./vol.) ethanol, incubated for 12 hr in PBS with 1 mg/mL RNase A, and stained for 1 hr with 5 mg/mL propidium iodide (Sigma). After sonication, DNA content in the sample was analyzed using a FACSCalibur flow cytometer (Becton Dickinson).

Chromatin immunoprecipitation

Chromatin immunoprecipitation was carried out as described in [69], with slight modifications. In brief, 50 mL of exponential cell cultures were fixed with 1% formaldehyde for 15 min at room temperature and with rotation. Crosslinking reaction was stopped by adding 2.5 mL of 2.5 M glycine and incubated for 5 min at room temperature. For cell extract preparation, pellets were resuspended in 300 μL of lysis buffer (50 mM HEPES-KOH (pH 7.5), 140 mM NaCl, 1 mM EDTA (pH 8), 1% Triton X-100, 0.1% sodium deoxycholate) supplemented with protease inhibitors (1x Complete Protease Inhibitor Cocktail (Roche) and 1 mM PMSF), and then lysed in a Multi-Beads Shocker (Yasui Kikai Corporation) for 60 min at 4°C, alternating pulses of 60 s at 2500 rpm with 60 s rest. The whole extract was sonicated in a Bioruptor for 20 min, alternating 30 s high-intensity pulses with 30 s rest, in order to fragment the chromatin. Samples were centrifuged for 15 min at 13000 rpm and 4°C to eliminate cell debris. 20 μL of supernatant were processed as input and 200 μL were immunoprecipitated. For the immunoprecipitation, 5 μL of anti-Pk antibody SV5-Pk1 (Bio-Rad) were used. After overnight incubation at 4°C with rotation, 50 μL of Protein A-Sepharose® CL-4B beads (GE Healthcare), previously equilibrated in lysis buffer, were also added to the sample, which was incubated for another 2-4 hr at 4°C. After the incubation, the sample was washed twice with lysis buffer, another two times with washing buffer (10 mM Tris-HCl (pH 8), 1 mM EDTA, 250 mM LiCl, 0.5% Igepal and 0.5% Triton X-100), and finally one last time with TE (10 mM Tris-HCl (pH 8), 1 mM EDTA). Chromatin

was eluted in 60 μL TE supplemented with 1% SDS for 10 min at 65°C. 20 μL of chromatin and input samples were treated with 20 μL of fresh TE plus 1% SDS and 1.2 μL of 50 mg/mL pronase for 2 hr at 42°C, and then de-crosslinked for 6 hr at 65°C. Next, 360 μL of TE, 10 μL of 10 mg/mL glycogen and 35 μL of 5 M LiCl were added to the samples and mixed. The same volume of phenol-chloroform was used to clean the DNA. The supernatant was transferred to a new tube and 1 mL of 96% ethanol was added. Samples were incubated overnight at −20°C and then DNA was precipitated by centrifugation at 12000 g and 4°C. DNA pellets were washed with 70% ethanol, dried, and resuspended in 40 μL TER (20 μL of 10 mg/mL RNaseA in 1 mL of TE). Samples were incubated at 37°C for 1 hr. RNase was diluted by adding 160 μL of TE. Inputs were diluted 1:25. Real-time quantitative PCR was performed using iTaq universal SYBR Green (Bio-Rad) in a 7500 Fast Real-Time PCR machine (Applied Biosystems). Oligonucleotide sequences for real-time PCR amplifications were originally described in [70, 71] and are shown in Table S5.

Quantification of rRNA transcription

For the analysis of RNA Pol I transcripts, 10 mL of culture were harvested, pelleted, and resuspended in 400 μL of TES buffer (10 mM Tris-HCl (pH 7.5), 10 mM EDTA, 0.5% SDS). An equal volume of phenol was added to the sample and, after agitation with a vortex, tubes were incubated for 45 min at 65°C. The sample was then incubated at 4°C for 5 min and centrifuged for 5 min at 13000 g and 4°C. The aqueous phase was transferred to a new tube, extracted again with an equal volume of phenol, and one last time with an equal volume of chloroform. The final aqueous phase was transferred to a new tube, mixed with 40 μL of 3 M Sodium Acetate (pH 5.2) and 1 mL of ethanol, and precipitated for 1 hr at −20°C. After centrifugation, the RNA pellet was washed with 70% ethanol, dried, and finally resuspended in 50 μL diethylpyrocarbonate-treated H_2O. Quantitative RT-PCR reactions were performed in a 7500 Real-Time PCR System (Applied Biosystem). To this end, 2 μg of total RNA were first treated with Dnase I (Invitrogen), and cDNA was synthesized using the SuperScript III Reverse Transcriptase kit (Invitrogen). Then, quantitative PCRs were carried out using a 1:5 dilution of the cDNA sample, the primers shown in Table S5, and iTaq Universal SYBR® Green Supermix. Fluorescence values, Ct values and all quantifications were obtained using the 7500 Real-Time PCR Software v2.06.

Genomic DNA extraction

Genomic DNA was prepared starting from 5 mL of an exponential cell culture. Cells were first pelleted by centrifugation for 5 min at 2500 g, washed with distilled water, and finally resuspended in 0.9 M sorbitol, 0.1 M EDTA (pH 8), 1% β-mercaptoethanol and 0.5 μg/μL Zymolyase 20T. The mixture was then incubated for 60 min at 37°C. The generated spheroplasts were pelleted by centrifugation for 1 min at 700 g, and lysed in 250 μL of 20 mM EDTA, 50 mM Tris-HCl (pH 8) and 0.5% SDS for 30 min at 65°C. Extracts were cleared at 4°C by adding 85 μL of 5 M potassium acetate (pH 4), and cell debris were pelleted by centrifugation for 15 min at 13000 g. After this, 1.2 mL of 96% ethanol were added to the supernatant, and the mixture was incubated for 15 min at −20°C. Genomic DNA was precipitated by centrifugation for 15 min at 13000 g, and the pellet was resuspended in 300 μL of TE buffer and treated with 20 μg RNase A for 1 hr at 37°C. After RNase treatment, 300 μL of a phenol:chloroform:isoamyl alcohol (25:24:1) solution were added, and the mixture was gently swirled and centrifuged for 15 min at 13000 g. The aqueous phase was transferred to a new tube, and 10 mM NaCl and 2 volumes of 96% ethanol were added to the solution. After 30 min at −20°C, DNA was pelleted by centrifugation for 15 min at 13000 g. The pellet was dried and finally dissolved in TE buffer. The concentration of the extracted genomic DNA was determined by spectrophotometry.

Estimation of rDNA copy number in genomic DNA

Total DNA was diluted to 25 ng/μL. qPCR reactions were carried out in triplicate on an Applied Biosystem 7500 Real-Time PCR System. Each amplification reaction contained 10 μL iTaq Universal SYBR Green Supermix (Bio-Rad), 2 μL DNA template and 500 nM of each primer in 20 μL total reaction volume. PCR efficiency for each primer was determined from a standard curve. The number of copies of each specific locus per strain genome was estimated by normalizing the absolute copy number of the target (the NTS2 and ITS2 regions of the rDNA locus or the *TUB2* control gene) to the reference gene *PDA1*. Primers for the amplification of the previous DNA sequences are described in Table S5.

QUANTIFICATION AND STATISTICAL ANALYSIS

Details of the statistical analysis of the experiments, including the specific measure used to estimate the variation within each group of data and the exact value of n, can be found in the figure legends.